ARL 63-167

INVESTIGATIONS OF BALLISTIC-PISTON AND LIQUID DRIVEN PISTON COMPRESSORS FOR THE PRODUCTION OF HIGH TEMPERATURE AND HIGH DENSITY GASES

JOHN E. MINARDI
ROBERT B. SCHWARTZ

RESEARCH INSTITUTE
UNIVERSITY OF DAYTON
DAYTON, OHIO

AUGUST 1963

AEROSPACE RESEARCH LABORATORIES
OFFICE OF AEROSPACE RESEARCH
UNITED STATES AIR FORCE

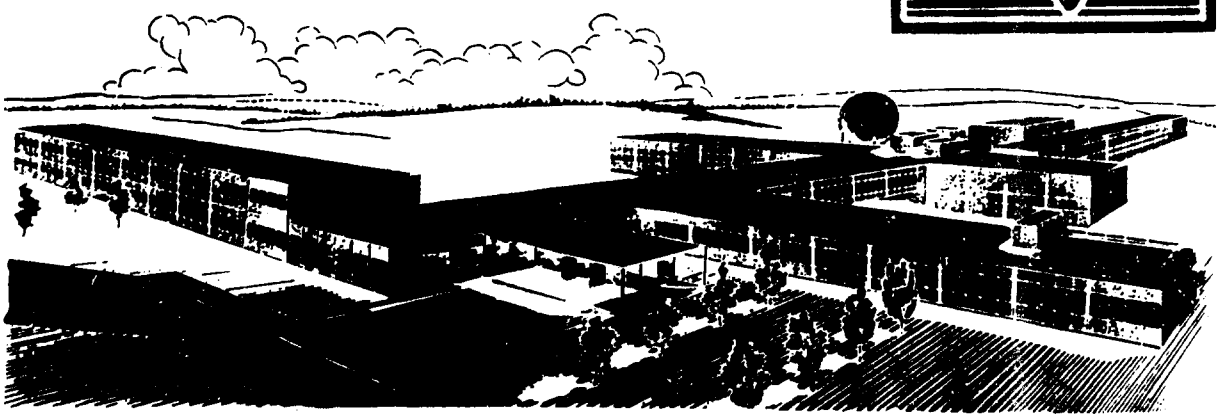

NOTICES

When Government drawings, specifications, or other data are used for any purpose other than in connection with a definitely related Government procurement operation, the United States Government thereby incurs no responsibility nor any obligation whatsoever; and the fact that the Government may have formulated, furnished, or in any way supplied the said drawings, specifications, or other data, is not to be regarded by implication or otherwise as in any manner licensing the holder or any other person or corporation, or conveying any rights or permission to manufacture, use, or sell any patented invention that may in any way be related thereto.

- - - - - - - - -

Qualified requesters may obtain copies of this report from the Armed Services Technical Information Agency, (ASTIA), Arlington Hall Station, Arlington 12, Virginia.

- - - - - - - - - -

This report has been released to the Office of Technical Services, U.S. Department of Commerce, Washington 25, D.C. for sale to the general public.

- - - - - - - - - -

Copies of ARL Technical Documentary Reports should not be returned to Aeronautical Research Laboratory unless return is required by security considerations, contractual obligations, or notices on a specific document.

ARL 63-167

INVESTIGATIONS OF BALLISTIC-PISTON AND LIQUID DRIVEN PISTON COMPRESSORS FOR THE PRODUCTION OF HIGH TEMPERATURE AND HIGH DENSITY GASES

John E. Minardi
Robert B. Schwartz

University of Dayton Research Institute
Dayton, Ohio

August 1963

Contract No. AF 33(657)-8975
Project No. 7116
Task No. 7116-01

Aerospace Research Laboratories
Office of Aerospace Research
United States Air Force
Wright-Patterson Air Force Base, Ohio

FOREWORD

This interim technical documentary report was prepared by the University of Dayton Research Institute, Dayton, Ohio, on Air Force Contract AF 33(657)-8975 for the Aerospace Research Laboratories, Office of Aerospace Research, United States Air Force. This contract was initiated under Project No. 7116 and Task No. 7116-01, "Internal Flow Research." The work was administered under the direction of the Fluid Dynamics Research Laboratory with Mr. Maurice O. Lawson as the ARL Project Engineer.

The able assistance and cooperation of the members of the Aerospace Research Laboratory, and in particular the efforts of Mr. Lawson, Dr. Hans J. P. von Ohain and Dr. Roscoe H. Mills are appreciated and hereby acknowledged.

The work described herein was conducted in the period 15 June 1962 to 14 June 1963.

ABSTRACT

Research on systems for the production of high temperature and high density gases is being conducted by the University of Dayton Research Institute to determine the feasibility of various pressure energy exchange apparatus to produce isolated high temperature and high pressure gas. The subject of this technical note is the theoretical analysis and experimental test program conducted to gain insight into the operation of ballistic-piston compressors, and the continuation of effort toward the development of liquid driven gas compression systems.

The analysis adopted to determine the parameters affecting the maximum performance of the ballistic-piston compression process has been divided into two cases. A heavy piston treatment, which considers the charge gas compression to be polytropic, is presented for compressions in which the irreversibilities induced into the charge gas by pressure waves may be considered negligible. If the entropy increases associated with these waves are not negligible a light piston analysis is required.

The results, of the analytical developments corroborated by empirical data, indicate that the peak performance of the heavy piston compression process is independent of piston mass whereas for the light piston compression the piston mass is a significant variable. The data also clearly demonstrate the degradation of peak performance due to piston frictional effects.

The experimental results of the liquid driven piston system, in which the charge gas is rapidly compressed as it decelerates a high speed column of water, have demonstrated that pressures in excess of water hammer can be achieved. Hence, it is seen that the piston, in addition to providing a means of separating the liquid driver and charge gas, enables higher pressures to be achieved than the impact pressure in the driver fluid.

The results of analytical studies which were directed towards tailoring a tube, to eliminate Taylor instability, for use in systems in which mechanical separation is not desirable are also discussed in this report.

TABLE OF CONTENTS

LIST OF FIGURES

LIST OF FIGURES CONT'D.

LIST OF FIGURES CONT'D.

LIST OF SYMBOLS

A	area
a	speed of sound in gas
C_v	specific heat at constant volume
c	coefficient of kinetic friction; wave velocity
D	tube diameter
d	O-ring cross sectional diameter
f	friction force
i	interface location
KE	kinetic energy
ℓ	length
M	mass
n	polytropic exponent
P	pressure
q	dynamic pressure
$\bar{q}$	q/P_c
R	KE/WK_c
S	slope; residual stress
s	speed of sound in liquid
T	temperature
t	time
t'	normalized time
U	normalized velocity
u	velocity
V	volume
v	specific volume
W	weight; weight of charge gas

LIST OF SYMBOLS CONT'D.

WK	work
X	normalized length
x	variable length
Y	$A_e/A(i)$
γ	ratio of specific heats
λ	ratio of volume to V_o
π	ratio of pressure to P_o
π_{df}	effective driver pressure ratio (driver pressure ratio adjusted for piston frictional effects)
π_{ef}	equilibrium pressure ratio adjusted for piston frictional effects
ρ	density
τ	ratio of temperature to T_o
ν	V_i/V_o

Subscripts

bd	condition of interface breakdown
c	charge gas; compression chamber; compression criteria
d	driver fluid
E	energy or expansion criteria
e	entrance; effective; equilibrium
i	interface
L	liquid
m	condition at maximum pressure
o	initial charge gas condition; except u_o = initial velocity
p	piston
R	residual

LIST OF SYMBOLS CONT'D.

Subscripts Cont'd.

r	condition after reflected wave
s	condition after reflected shock; signaling criteria
s1	conditions after first shock wave
T	tank (driver storage vessel)
t	tube
wh	water hammer condition
x	condition before wave passage
y	condition after wave passage

SECTION I

INTRODUCTION

As a result of recent advances in technology, the need for producing gases with extremely high values of temperature, density, and pressure has become increasingly important in many fields of endeavor. Many methods are currently available for producing high temperature gases, but associated with most of these techniques are low values of density. Thus, only a restricted area on the p-v-t surface can be explored in gas property investigations. Similarly the scope of investigations which utilize high temperature and high density gases is limited.

The ballistic-piston compressor, however, is capable of yielding high values of density as well as temperature and consequently offers increased possibilities for study and application. These compressors have been employed advantageously to indagate gas properties in several countries and have found application as a driver source of high temperature and high density gas for a hypersonic tunnel, a shock tube, and for light gas guns.

The University of Dayton has been investigating the ballistic-piston compressor in order to understand its operation and develop theoretical relations for predicting performance. Equations have been developed for the prediction of the peak pressures and temperatures which can be achieved with the free-piston compressor. The development of these relations and the supporting experimental program are described in this report.

The continuation of effort towards the development of liquid driven gas compression systems is also discussed in this report. These systems were contrived to investigate the performance characteristics of systems which utilize the kinetic energy of a liquid column to compress an initially low pressure charge of gas. In addition to the test results of the liquid driven piston system, a theoretical analysis of a tube tailored to maintain a constant interface velocity during the liquid to gas compression process is presented.

SECTION II

BALLISTIC-PISTON COMPRESSION PROCESS

The ballistic-piston compressor (also referred to in the literature as the free-piston compressor) utilizes the work of expansion of a high pressure driver gas to accelerate a piston into the initially low pressure charge gas. The charge gas is rapidly compressed, as it decelerates the piston, increasing both the temperature and pressure of the charge gas. The basic components of this system are depicted schematically in Figure 1.

The University of Dayton Research Institute has been investigating ballistic-piston compressors in order to understand their operation and develop theoretical equations for predicting performance. Theories developed for the prediction of the peak performance of the ballistic-piston compressor and the supporting experimental program are the subject of this section.

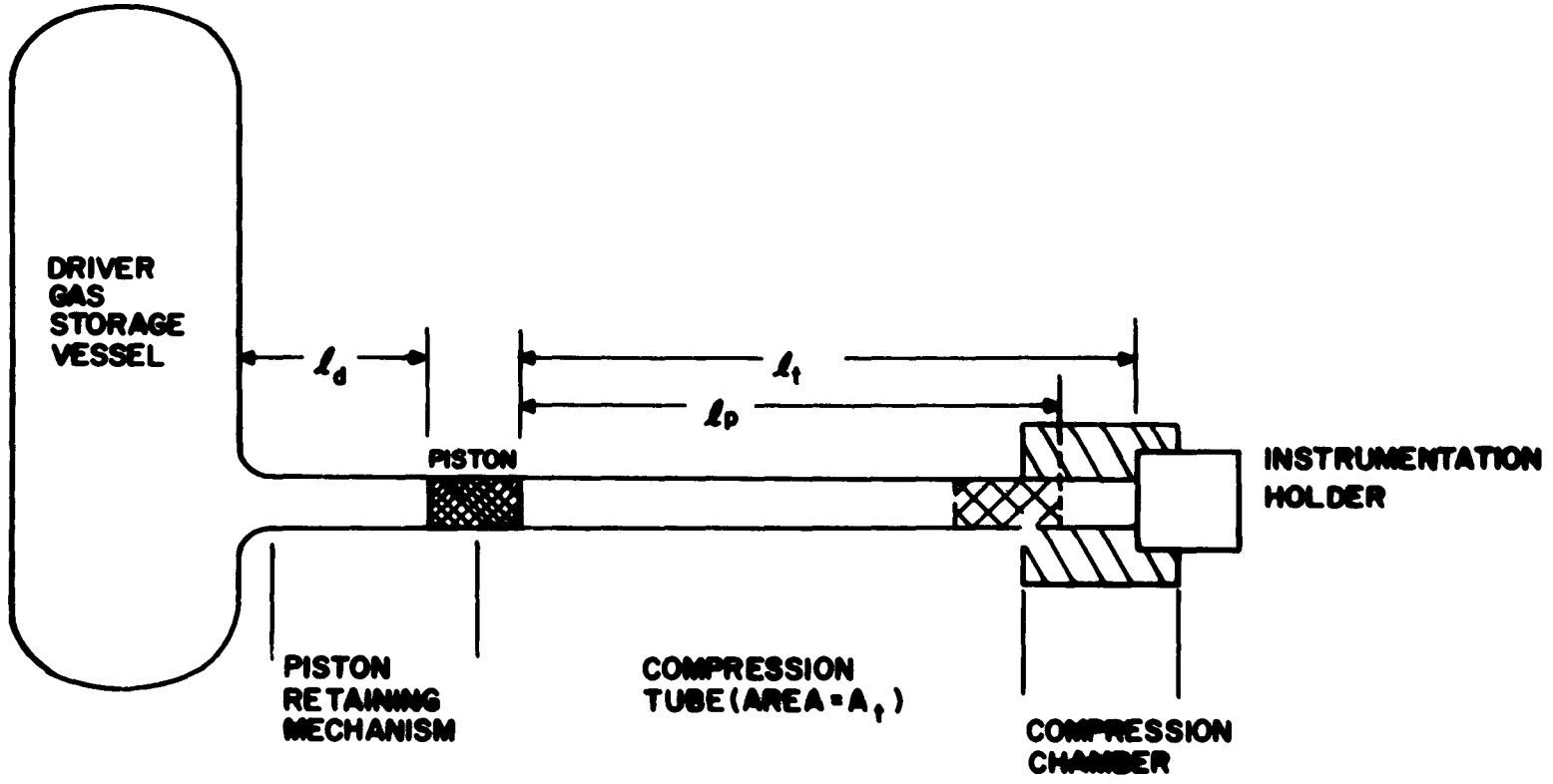

Figure 1 Schematic Diagram of Ballistic-Piston Compressor

A. THEORETICAL CONSIDERATIONS

The analysis adopted to determine the parameters affecting the maximum performance of the free-piston compression process has been divided into two cases. A heavy piston treatment, which considers the charge gas compression to be polytropic, is presented for compressions in which the irreversibilities induced into the charge gas by pressure waves may be considered negligible. If the entropy increases associated with these waves are not negligible a light piston analysis is required.

1. General Considerations

a. Ideal Model

In order to illuminate the salient features of the ballistic-piston compressor an idealized model will first be presented. The free-piston compressor (see Figure 1) consists of a driver storage vessel, containing a gas at pressure P_d; a piston, of weight W_p; and a long barrel (length ℓ_t and area A_t), containing the charge gas at pressure P_o, temperature T_o, and weight W. Upon release, the piston travels a distance ℓ_p and compresses the charge gas (specific heat at constant volume, C_v, and specific heat ratio γ) to a peak pressure P_m and temperature T_m. With the assumptions that the compression process is adiabatic, the volume of driver gas is much larger than the charge gas volume (i.e. P_d = constant), and all the work from the driver gas is absorbed by the charge gas, the first law of thermodynamics yields

$$P_d \ell_p A_t = C_v W(T_m - T_o). \tag{1}$$

Noting that $\ell_p \doteq \ell_t$ for the cases of interest and setting $\pi_d = P_d/P_o$, Eq (1) yields,

$$\tau_m = T_m/T_o = (\gamma - 1)\pi_d + 1. \tag{2}$$

Hence, for an adiabatic compression the final temperature, τ_m, is determined from Eq (2) regardless of the peak pressure, π_m, or the particulars of the compression process. Figure 2 is a PV diagram on a logarithmic scale, of a diatomic gas ($\gamma = 1.4$), where the pressure and specific volume are normalized by the initial values of pressure, P_o, and specific volume, v_o, respectively. For a given driver pressure ratio, π_d, the final state is restricted, by Eq (2), to lie somewhere on a particular temperature ratio line, τ_m, (such as the line marked S - V of Figure 2). Further, in view of the second law of thermodynamics, as applied to an adiabatic compression, the end state must lie to right of the line O - S.

To gain some insight into the particular processes that occur when the piston weight is varied, consider a model where the piston is accelerated in a separate tube until the kinetic energy is equal to $P_d \ell_p A_t$; at this point the driver pressure drops to zero and the piston impinges on the charge gas. If for the given energy (i.e. a fixed value of P_d) the piston mass M_p is large and the velocity u small, the peak state would approach the point S of Figure 2; if u is large and M_p small, due to shock heating, the peak state would approach the point V. In the limiting case $M_p = \infty$ and u = 0, the process would be reversible and adiabatic, hence, the point S would be achieved (O - S is an

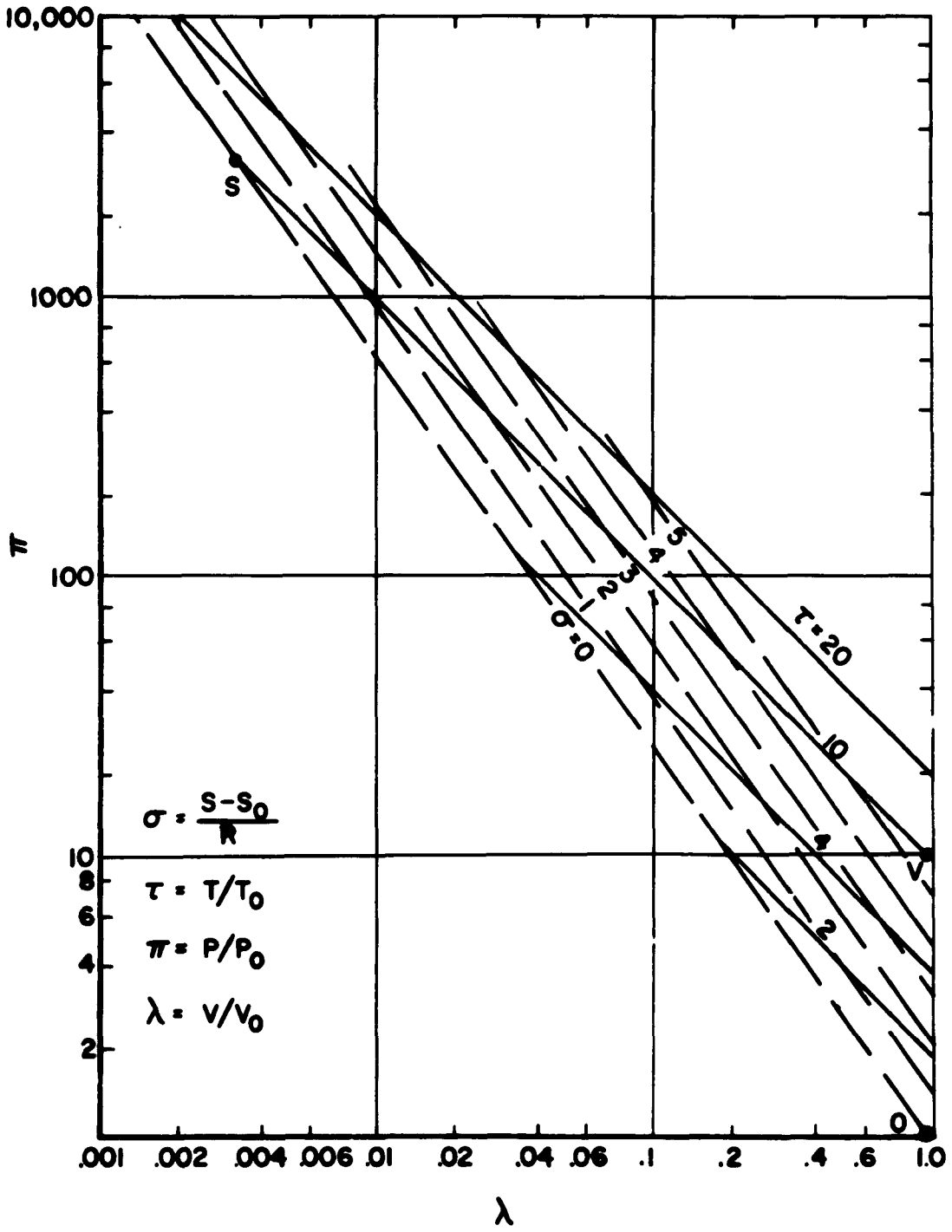

Figure 2 Pressure-Volume Diagram Indicating the Range of States which Can Be Reached with the Ideal Model of the Ballistic-Piston Compressor by Varying the Piston Mass

isentropic process). In the other limiting case, $M_p = 0$ and $u = \infty$, the point V would be obtained. Therefore, for the adiabatic model thus far discussed, the final state is restricted to lie between the points S and V; further, no single theoretical model (except for a complete characteristic treatment) could be expected to represent the final state over the complete spectrum of piston weights.

Although the attainment of the limiting cases cannot be taken too seriously, it should be noted that the point S can, for practical purposes, be achieved, while the point V could not. Nevertheless, this simple model demonstrates the versatility which can be achieved with a ballistic-piston compressor by the simple expedient of varying the piston mass.

There exists, of course, other phenomena which degrade the performance indicated by Eq (2): friction acting on the piston; heat losses, which may be more significant in the heavy piston case; the pressure behind the piston may drop significantly below P_d in the light piston case; and for light pistons, shocks are induced into the portion of the driver gas in the tube and represents an energy loss to the charge gas.

b. Characteristic Solution

In an attempt to understand the degradation of the performance of the air driven piston system as compared to the theoretical values determined by Eq (22) of Reference 1 (see Eq 6a), it was deemed advisable to program a characteristic solution of the problem on a digital computer. It was felt that an energy storage in the driver air which entered the tube might account for a great deal of the degradation. However, this was shown to be a false assumption.

The model used consisted of an infinite reservoir, a straight closed end tube, and a piston located a short distance from the inlet end of the tube. In order to make the problem tractable, a simplified method for coalescing compression waves at the wall was used, and it was further assumed that the Mach number at the open end would be low enough so that an approximation to the steady flow equations for a compressible fluid would be adequate. Although the program is not completely general, an examination of the results will determine the validity of the simplifications for a particular problem.

The problem was separated into several different wave interactions which were:

(a) wave interaction with open end,
(b) wave interaction with closed end,
(c) wave interaction with the piston, and
(d) right running waves interacting with left running waves.

The general equations for the waves are:

$$\frac{P_y}{P_x} = 1 + \gamma \frac{u_y - u_x}{a_x} \qquad \text{(Right running wave)} \qquad (3)$$

and

$$\frac{P_y}{P_x} = 1 - \gamma \frac{u_y - u_x}{a_x} \qquad \text{(Left running wave).} \tag{4}$$

At the wall the equation for the left running wave along with the boundary condition

$$u_y = 0$$

was used.

At the tank end the equation for the right running wave along with the steady flow equation,

$$\frac{P_T}{P_y} = 1 + \frac{\gamma}{2}\left(\frac{u_y}{a_o}\right)^2 , \tag{5}$$

were used along with the conditions that the velocity and pressure, given by the steady flow equation, be equal to those given by the right running wave equation. The steady flow equation above gives an error of less than 1% for $u_y/a_o = 0.4$ and less than 2% for $u_y/a_o = 0.5$.

When the original waves were sent out from the piston, it was assumed that the piston trajectory resulted from a constant acceleration until either the reflected wave from the wall or the open end returned to the piston. At this time the wave would be reflected from the piston, and the velocity behind the wave was set equal to the current piston velocity. Also, a new wave would eminate from the opposite side of the piston. The pressure behind these two waves would determine a new acceleration of the piston which would prevail until another wave would impinge upon the piston. This procedure was repeated until the piston velocity became zero.

The program considered only one wave coming from the wall and the open end at any time, and a procedure was used to determine which wave impinged on the piston first. (If both waves arrived at approximately the same time, it was assumed that they arrived at the same time to prevent a compression wave from overtaking the preceding compression waves.)

The interaction of a right running wave and a left running wave was determined from the two equations and the conditions that the pressures and velocities are equal after the wave interaction.

The original program was run neglecting friction and the peak pressure obtained was considerably greater than the experimental values obtained for similar conditions, as shown in Figure 3. At this time, a term was added to account for piston friction; the result of this run is also compared with the experiment in Figure 3. In Figure 3, the time of the peak pressure from experiment was set equal to the time of the peak pressure from calculations, since no absolute time base was obtained with the experimental data. Similar results were obtained at various other driver pressure ratios and values of the piston weight parameter. Thus, the results of this study indicate that the major degradation of performance is the result of piston friction.

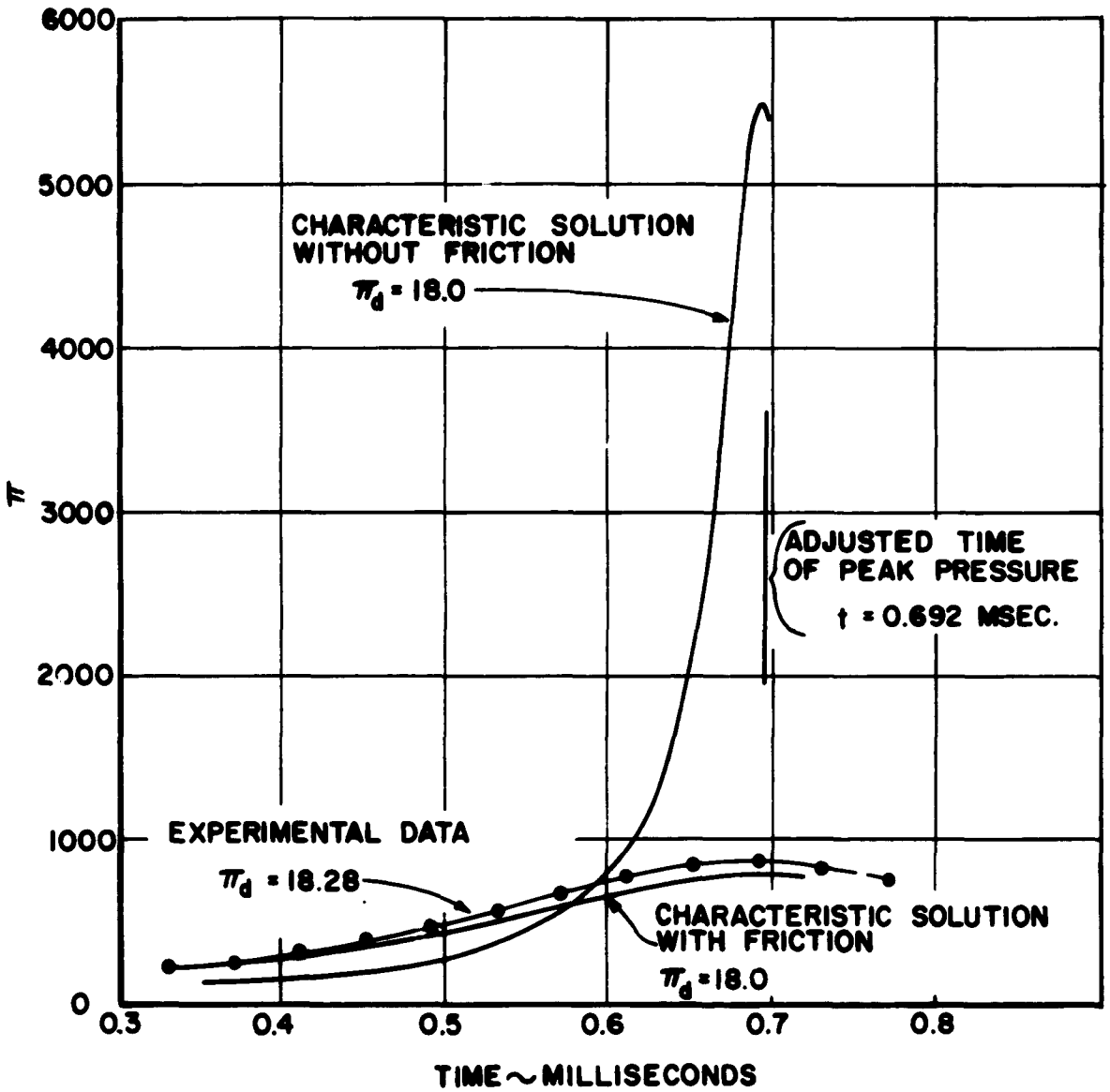

Figure 3 Comparison of a Characteristic Solution for the Ballistic-Piston Compressor, with and without Friction Effects, with Experimental Data

2. Heavy Piston Theory

Consider a simple energy balance neglecting friction. Further, assume the compression to be polytropic and the driver pressure constant. The work of expansion of the driver gas is equal to the work of compression of the charge air thus, as in Reference 1,

$$\pi_d = \frac{(\pi_m)^{\frac{n-1}{n}} - 1}{(n-1)\left[1 - (\pi_m)^{-1/n}\right]}, \tag{6a}$$

where n = polytropic exponent.

Since the final charge pressure ratio is much greater than unity, in the range of interest, a useful approximation to Eq (6a) is

$$\pi_m = \left[1 + (n-1)\pi_d\right]^{\frac{n}{n-1}}, \tag{6b}$$

which agrees with Reference 2 if n is replaced by the ratio of specific heats γ. The peak pressures obtained experimentally are considerably lower than predicted by Eq (6b), as was expected, since the results of the characteristic solution study indicated that a major degradation of performance results from piston frictional effects. Therefore, the momentum equation for the heavy piston case is

$$M_p \frac{du}{dt} = P_d A_t - P_c A_t - f, \tag{7}$$

where f is the force resulting from piston friction. The frictional force depends on the particular piston design as well as the coefficient of kinetic friction, c. For the piston designs used for this study, two O-rings were used for sealing; it was assumed that the friction force results from O-ring contact with the walls. The normal force acting on the wall consists of a residual stress, S, caused by O-ring squeeze and a stress resulting from the pressure the O-ring seals. This latter stress is assumed to be equal to the pressure which the O-ring seals (P_d on the driver side and P_c on the charge gas side). If the O-rings have an overall diameter D and a cross-sectional diameter d the friction force is

$$f = c\pi Dd\,(P_d + P_c + 2S). \tag{8}$$

Combining Eqs (7) and (8), and normalizing the variables, yields

$$U \frac{dU}{dX} = \frac{W}{\gamma W_p}\left[(1 - 4c\frac{d}{D})\pi_d - (1 + 4c\frac{d}{D})\pi_c - 8c\frac{d}{D} \cdot \frac{S}{P_o}\right], \tag{9}$$

where X is a length in units of ℓ_t and U is in units of the initial speed of sound in the charge gas, a_o.

Equation (9) can be integrated with the aid of the following assumptions which are valid for a heavy piston:

(a) π_d is constant,
(b) π_c is a function of X only, in particular, the compression process is polytropic, i.e.
$\pi_c = (1 - X)^{-n}$, and
(c) the charge gas acts as a perfect gas.

The result of the integration is

$$\frac{U^2}{\Sigma} = \frac{W}{\gamma W_p} (1 + 4c\frac{d}{D})\left[\pi_{df} X + \frac{(1 - X)^{1-n} - 1}{1 - n}\right], \tag{10}$$

where the effective driver pressure ratio π_{df} is given by the equation

$$\pi_{df} = \frac{1 - 4c\frac{d}{D}}{1 + 4c\frac{d}{D}} \pi_d - \frac{8c\frac{d}{D}\frac{S}{P_o}}{1 + 4c\frac{d}{D}}. \tag{11}$$

Replacing X in terms of π_c and noting that the maximum value of π_c (i.e. π_m) occurs when U = 0 gives

$$\pi_{df} = \frac{\pi_m^{\frac{n-1}{n}} - 1}{(n - 1)(1 - \pi_m^{-1/n})}, \tag{12}$$

or for $\pi_m >> 1$,

$$\pi_m = \left[1 + (n - 1)\pi_{df}\right]^{\frac{n}{n-1}}. \tag{13}$$

Therefore, from Eqs (6b), (11) and (13), π_{df} is the value of the driver pressure adjusted for the effects of friction acting on the piston; further, Eq (13) is obviously independent of the piston weight parameter, $\gamma W_p/W$.

With the assumption of a polytropic process the temperature can be determined immediately from Eq (13), which yields

$$\tau_m = 1 + (n - 1)\pi_{df}. \tag{14}$$

Data and statements, given in References 2, 3 and 4, indicate that the peak pressure is influenced by the parameter $\gamma W_p/W$ eliminated from the analytic expression when the velocity was set equal to zero (see Eq (12). From Eq (10) we note that the parameter $\gamma W_p/W$ cannot influence the peak pressure (i.e. U = 0) as long as the right hand side of the equation is a function of X only. However, if either π_d or π_c is also (or only) a function of velocity it

would be probable that the parameter $\gamma W_p/W$ would influence the peak pressure. For high values of velocity, π_c would definitely be influenced by the velocity since strong shocks would eminate from the piston. Also, the pressure behind the piston might drop appreciably. (If the velocity of the piston exceeds the speed of sound in the driver it is obvious that the pressure behind the piston must be reduced.)

Qualitatively we see that Eq (12) should be satisfactory for relatively slow pistons, i.e. heavy pistons or $\gamma W_p/W$ large, and would not be satisfactory for relatively fast pistons, $\gamma W_p/W$ small.

3. Light Piston Theory

In the light piston case the piston will rapidly accelerate to its peak velocity, thus, a strong shock will propagate into the charge gas. The piston will continue at its peak velocity until the shock is reflected from the closed end and returns to the piston. As Reference 5 indicates, for a constant velocity piston, the major portion of the entropy increase occurs across the first two shocks, further, since the piston is light, it would decelerate rapidly, which would weaken (compared to the constant velocity case) all succeeding shocks.

The performance of the light piston was developed with the assumptions:

(a) the piston instantaneously achieves the equilibrium velocity, U_e, which is defined as the velocity the piston obtains when the acceleration is first zero in a compression tube of infinite length;

(b) a shock emanates from the piston, reflects from the end of the compression chamber, and returns to the piston, accounting for the total entropy increase;

(c) the friction is determined as in the heavy piston case;

(d) during the final compression, the pressure behind the piston remains constant at the equilibrium value, P_e;

(e) the final compression of the shock heated gas (properties π_s, τ_s and piston position X_s) is polytropic, i.e.

$$\pi_c = \pi_s \left(\frac{1 - X_s}{1 - X} \right)^n$$

(f) the charge gas acts as a perfect gas.

The peak pressure, using the above assumption, can be determined from Eq (9) by replacing π_d by π_e and integrating between the limits $U = U_e$ to $U = 0$ and $X = X_s$ to $X = X_{max}$. Integrating Eq (9) and rearranging yields

$$\pi_m = \pi_s \left[1 + \frac{(n-1)}{2\tau_s} \frac{\gamma W_p}{W} \frac{U_e^2}{\left(1 + 4c\frac{d}{D}\right)} + (n-1)\frac{\pi_{ef}}{\pi_s} \left\{ 1 - \left(\frac{\pi_m}{\pi_s} \right)^{-\frac{1}{n}} \right\} \right]^{\frac{n}{n-1}} \qquad (15)$$

where

$$\pi_{ef} = \frac{1 - 4c\frac{d}{D}}{1 + 4c\frac{d}{D}}\ \pi_e - \frac{8c\frac{d}{D}}{1 + 4c\frac{d}{D}}\left(\frac{S}{P_o}\right). \tag{16}$$

The terms π_s, τ_s, U_e and π_{ef} can be determined once π_d, c, and the geometry of the free-piston compressor are defined. The term $(1 - (\pi_m/\pi_s)^{-1/n})$ is approximately unity for large values of π_m/π_s, however, for smaller values Eq (15) can be iterated until a solution is found.

When the piston achieves the equilibrium velocity the acceleration of the piston is zero, hence,

$$P_e A_t = P_{s1} A_t + f,$$

where P_{s1} is the pressure after the first shock passes and, therefore, a function of U_e. This reduces to

$$\pi_e = \frac{1 + 4c\frac{d}{D}}{1 - 4c\frac{d}{D}}\ \pi_{s1} + \frac{8c\frac{d}{D}\frac{S}{P_o}}{1 - 4c\frac{d}{D}}. \tag{17}$$

The left hand term of Eq (17) can be determined from the geometry of the free-piston compressor.

For the design where the driver storage vessel diameter is large, such as is the case for the present equipment, the driver gas undergoes a steady expansion to Mach one, then an unsteady expansion to higher Mach numbers. Using the assumption of infinite driver volume, Figure 4 was constructed which has P_e/P_d as a function u/a_d, i.e. local pressure as a function of particle velocity. Figure 5 is a similar curve constructed for a normal shock, i.e. local pressure plotted as a function of particle velocity.

Utilizing Figures 4 and 5 along with Eq (17) the equilibrium pressure and velocity can be determined, Figure 6 is such a solution for the 33 Atmosphere Piston System with which a piston study was performed. Figure 7 is a working plot from which the temperature and pressure ratios can be determined after the reflected shock. Thus π_e and U_e can be determined from the intersections of Figure 6; τ_s and π_s from Figure 7 and π_{ef} from Eq (16). Substitution of these values into Eq (15) and iterating if necessary yields π_m. Data obtained in this manner along with the peak pressure ratio data obtained for the heavy piston theory is plotted as dashed lines in Figure 8.

However, if the driver storage vessel diameter were equal to the diameter of the compression tube, the expansion would be non-steady in its entirety. Utilizing data of Reference 6 and Figure 5 along with Eq (17) the equilibrium pressure and velocity can be determined as shown in Figure 9 for the non-steady expansion. Data for the solid lines of Figure 8 were obtained from Figures 9 and 7 and Eqs (16) and (15).

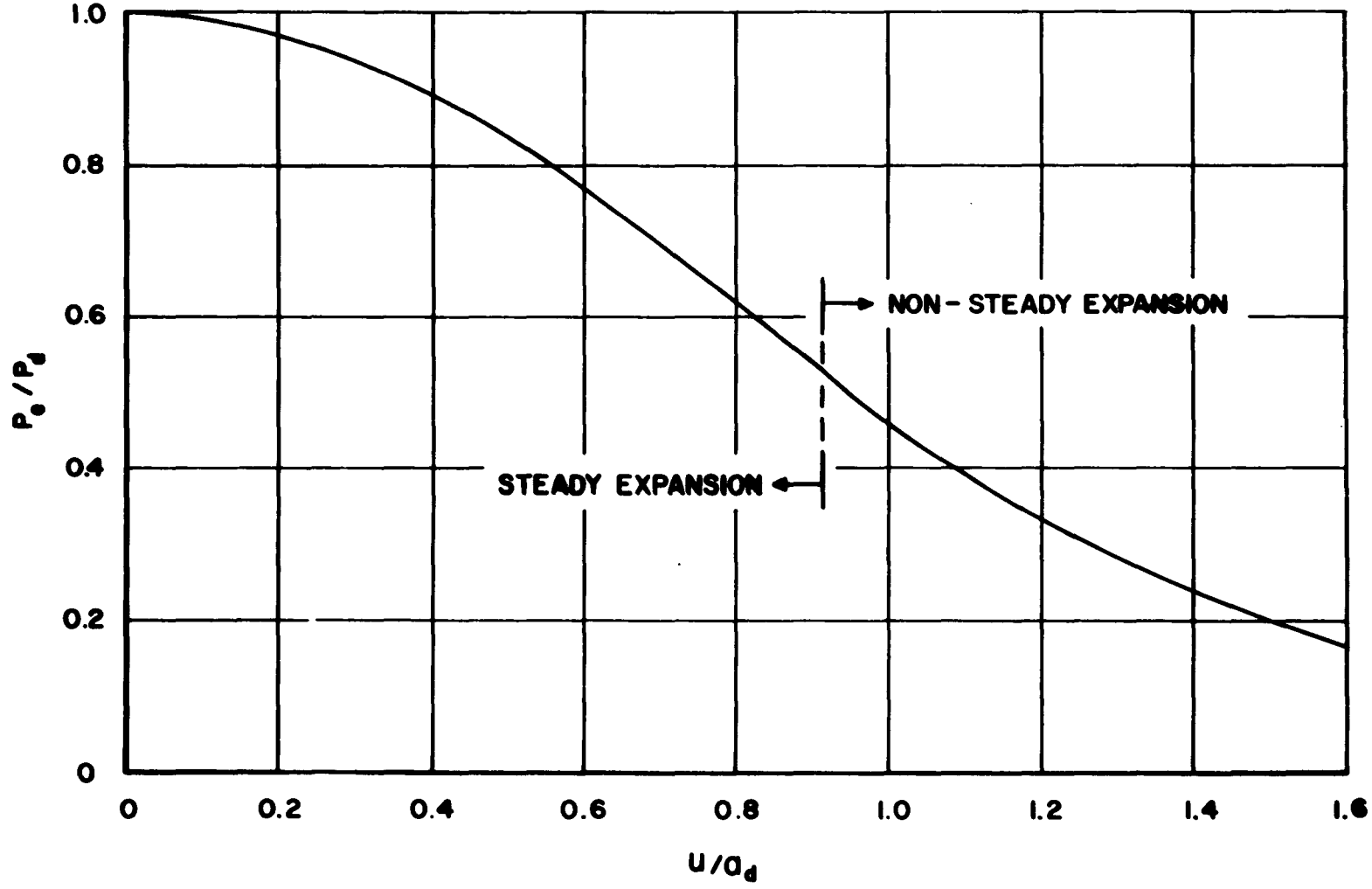

Figure 4 Local Pressure As a Function of Particle Velocity for Driver Gas Expansion in which the Storage Vessel Diameter Is Large Relative to the Tube Diameter

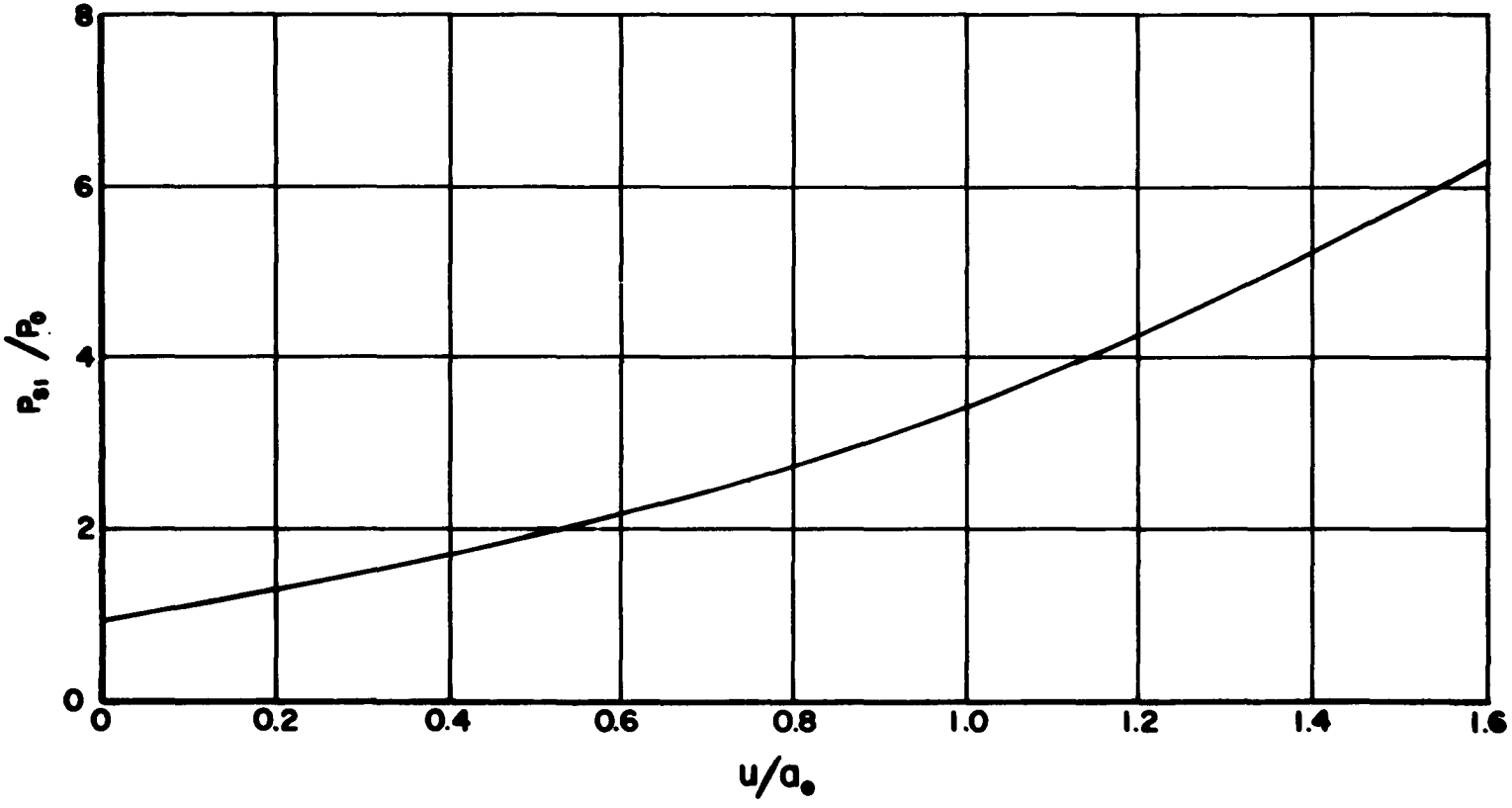

Figure 5 Pressure Ratio Across Normal Shock Wave As a Function of the Particle Velocity

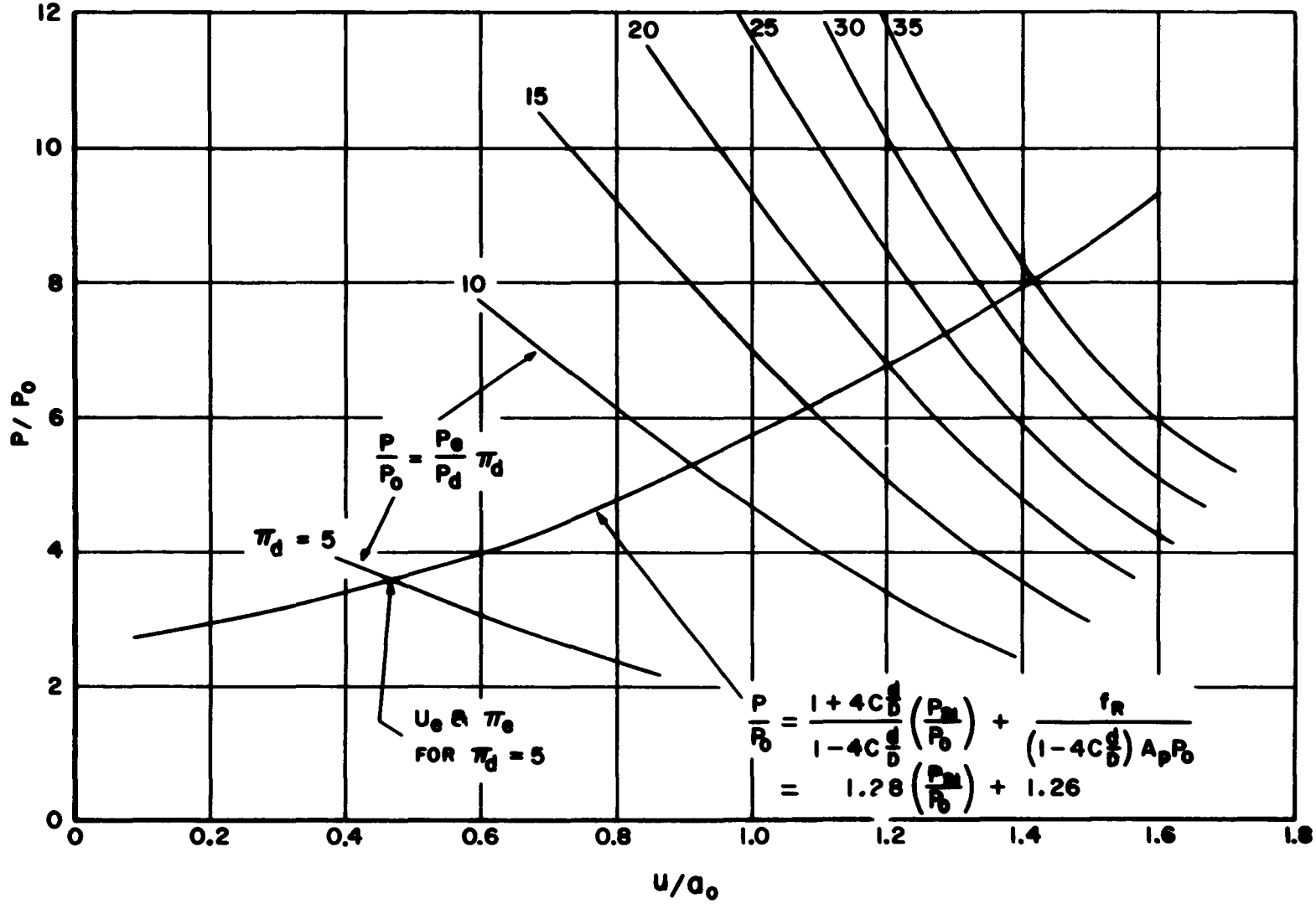

Figure 6 Determination of Equilibrium Pressure and Velocity for Case in which Driver Storage Vessel Diameter Is Large Relative to Tube Diameter.

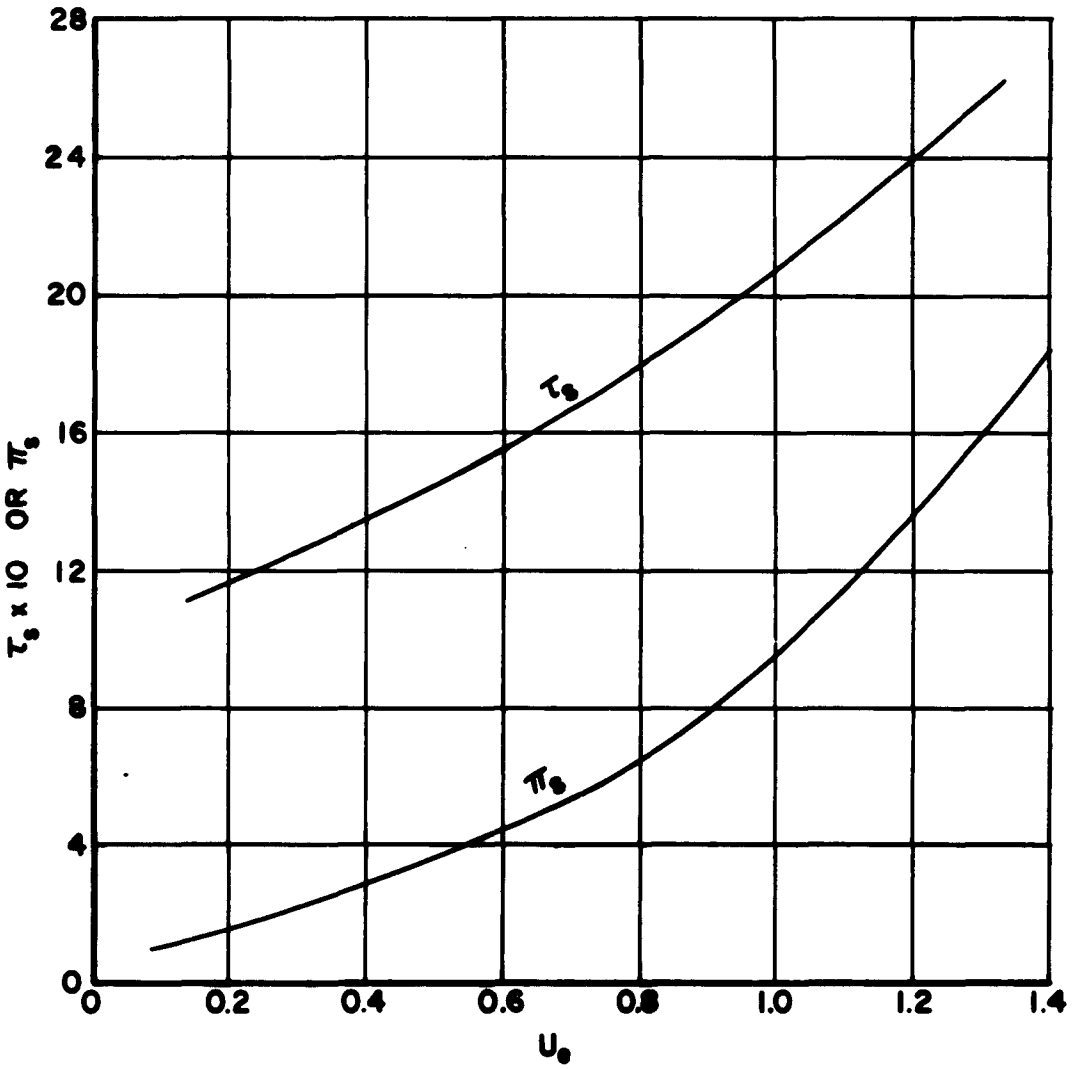

Figure 7 Temperature and Pressure Ratio Behind Reflected Shock Wave As a Function of Equilibrium Velocity.

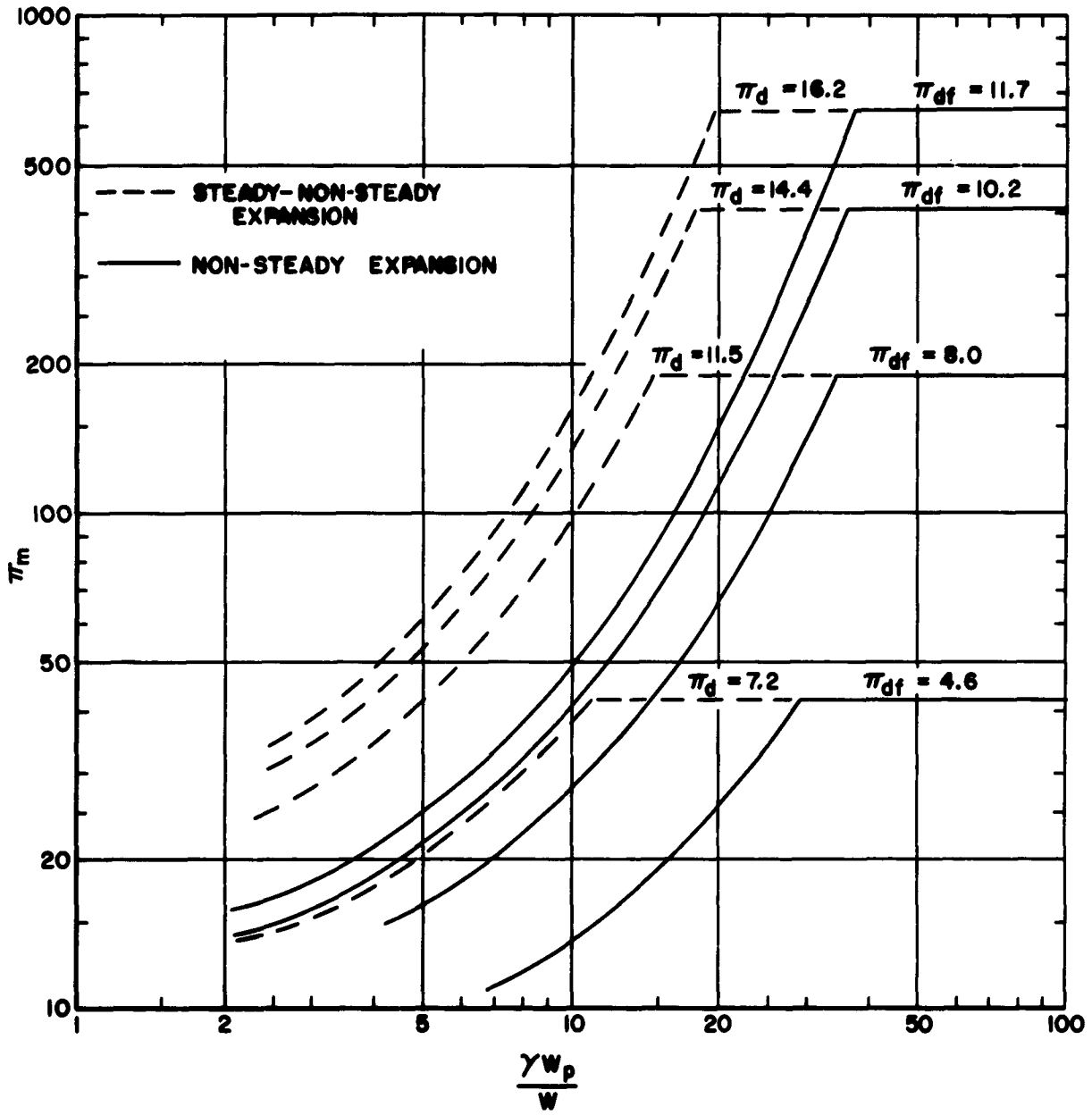

Figure 8 Light Piston Theory for the Two Driver Gas Expansions Discussed in Text.

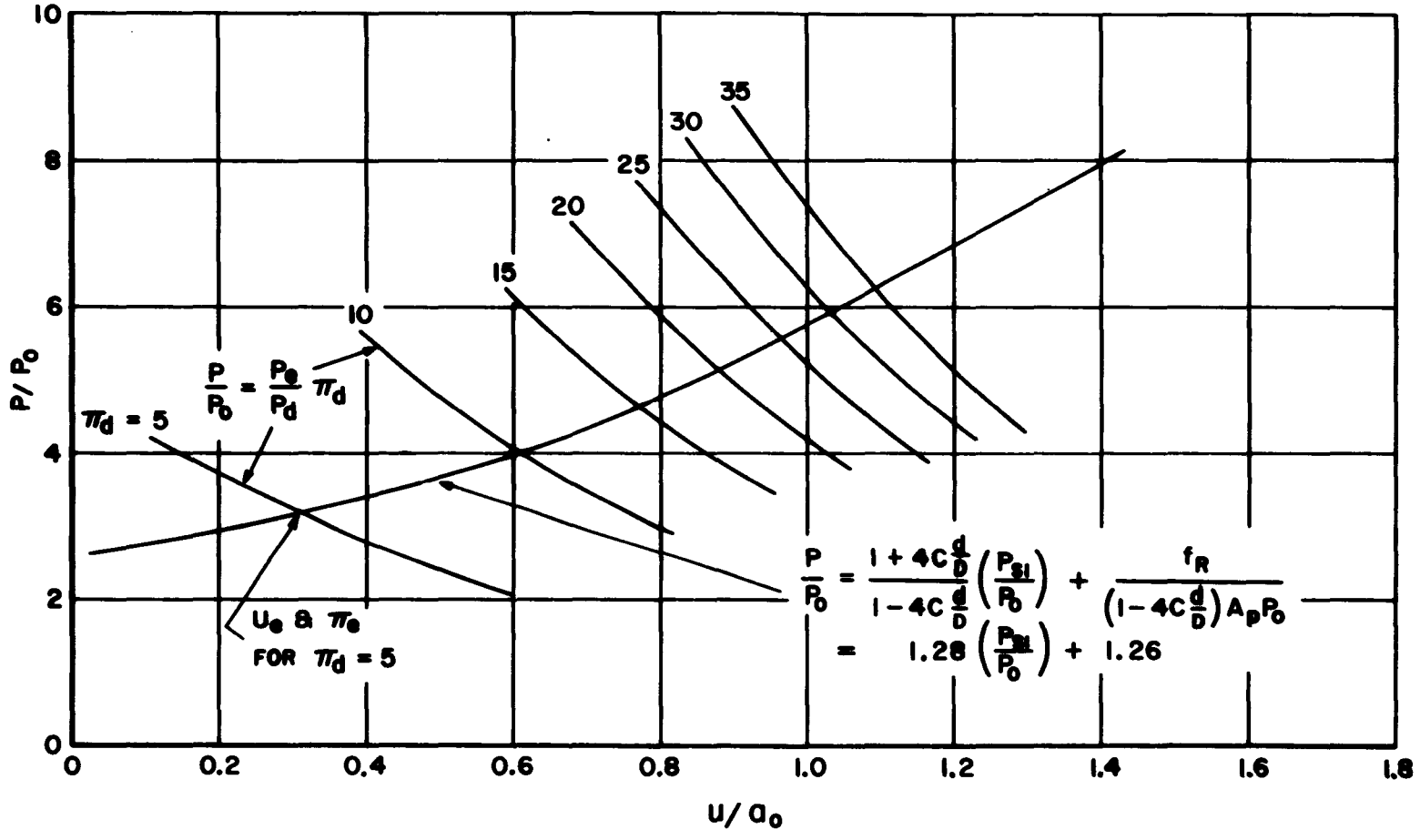

Figure 9 Determination of Equilibrium Pressure and Velocity for Case in which the Driver Storage Vessel Diameter Is Equal to Compression Tube Diameter.

A question arises, for the case of a diaphragm located away from the tank entrance in the tube, as to which of the above techniques should be employed. First let us consider the time, t_s, required for the shock to return to the piston. The distance Δx which the piston moves is given by the equation

$$\Delta x = \ell_t - \frac{RT_s}{A_t P_s} . \tag{18}$$

Hence the time is

$$t_s = \frac{\Delta x}{u_e} = \left[\ell_t - \frac{RT_s}{A_t P_s} \right] \frac{1}{u_e} \tag{19}$$

Normalizing Eq (11) yields

$$t'_s = \frac{t_s a_o}{\ell_t} = \left(1 - \frac{\tau_s}{\pi_s} \right) \frac{1}{U_e} . \tag{20}$$

Now consider the time t_E required for the first expansion wavelet to reflect from the bottle entrance back to the piston under the assumption that this wavelet travels at the speed of sound a_d in the driver gas. The distance d traveled by this wavelet is

$$d = 2\ell_d + \Delta x, \tag{21}$$

and the time required is

$$t_E = \frac{d}{a_d} = (2\ell_d + \Delta x) \frac{1}{a_d} . \tag{22}$$

Normalizing Eq (22) yields

$$t'_E = \frac{t_E a_o}{\ell_t} = \left(2 \frac{\ell_d}{\ell_t} + U_e t'_E \right) \frac{a_o}{a_d} , \tag{23}$$

or

$$t'_E = \frac{2 \frac{\ell_d}{\ell_t}}{\frac{a_d}{a_o} - U_e} . \tag{24}$$

If $t'_E \geq t'_s$ the equilibrium velocity should be determined from the non-steady expansion, this condition requires that

$$\frac{\ell_d}{\ell_t} \geq \left(1 - \frac{\tau_s}{\pi_s}\right)\frac{\left(\frac{a_d}{a_o} - U_e\right)}{2U_e} \tag{25}$$

For the 33 Atmosphere Piston System $\ell_d/\ell_t = 0.28$ and $a_d/a_o = 1$ for all tests, hence Eq (25) requires that $U_e > 0.51$ and $\pi_d > 6.7$. Thus empirical data with light pistons for the 33 Atmosphere Piston System should be compared to the solid curves of Figure 8.

In Reference 7 an expression is derived similar to Eq (15) with the assumptions that the final compression is isentropic, c = 0, and that the pressure behind the piston varies isentropically from P_e to the equivalent driver pressure gP_d (g depends on the area ratio A_d/A_t and varies from 1 to 1.89 for $\gamma = 1.4$: see Reference 8 pages 405-408). In view of the work reported in Reference 7 it appears that for large values of π_d the assumption of constant pressure π_e is poor, however, for the range of data presented here, Eq (15) is adequate and represents the correct trend for peak pressure as a function of $\gamma W_p/W$ and π_d.

With the assumptions used to develop the peak pressure, the peak temperature can be written

$$\tau_m = \tau_s \left(\frac{\pi_m}{\pi_s}\right)^{\frac{n-1}{n}} \tag{26}$$

From Eqs (11) and (16) we see that the parameter $8c(d/D)S/P_o$ influences the peak pressure for a given driver pressure and hence the peak pressure ratio is dependent on the value of the charge pressure P_o. The value of the initial charge pressure also plays a role in determining $\gamma W_p/W$ and caution in interpretation of the data must be exercised.

The value of S should be a kinetic value over the range of velocity experienced in a particular test. However, a constant value is probably adequate for the present theories of operation. The value, however, probably varies from shot to shot and will produce an unaccountable scatter in the data.

The value of the kinetic coefficient of friction c is also a function of velocity, but again a constant value of c will probably suffice.

B. DESCRIPTION OF COMPRESSORS

During the course of the experimental program tests were conducted utilizing two ballistic-piston compressors each of which can be represented by the same schematic shown in Figure 1. The basic dimensions and pressure capability of the 33 Atmosphere Piston System and 147 Atmosphere Piston System are given in Table I.

TABLE I

Pertinent Data on Piston Systems

Designation	Tube			Driver Vessel	
	ℓ_t in.	I.D. in.	Max. Press. atm	Volume ft^3	Max. Press. atm
33 Atm.	100	1	900	7.7	33
147 Atm.	64	1/2	2450	1.5	147

A driver storage vessel, diaphragm section, straight tube section, and compression chamber are the essential components of the 33 Atmosphere Piston System (see Figure 10). The diaphragm section consists of two diaphragm holders and the necessary valves and manifolding for initial pressurization of this section and for initiating the compression process. The function of the straight tube section is to initially contain the charge gas and after piston release to permit the driver gas to accelerate the piston before the charge gas resistance becomes appreciable. The instrumentation block inserted into the end of the compression chamber contains the instrumentation for measuring the charge gas properties during the compression process.

Figure 11 is a photograph of the 147 Atmosphere Piston System with the major components labeled. This relatively small high pressure piston system was constructed to corroborate and expand the range of the data obtained with the 33 Atmosphere Piston System.

The driver storage vessel for this system is a modified carbon dioxide cylinder. At the base of the cylinder a hole was machined and a special contoured outlet was fabricated to provide a connection from the tank to the piston holder.

A photograph of the piston holder assembly is shown in Figure 12. A plunger is free to slide through the cylinder wall of the holder body. This plunger is driven by a spring loaded air cylinder. When fully inserted it engages a groove in the center of the piston within the cylinder and restrains the piston from moving. O-rings on the pistons afforded the static-seal of the driver gas. Upon application of pressure to the air cylinder the plunger is retracted and the piston free to accelerate.

Teflon backed O-rings form the seal between the plunger and cylinder wall to prevent leakage of the driver fluid. Flanges welded to the ends of the cylindrical holder body provide connections with the tank connector and straight tube.

The 1/2 inch internal diameter, 1-1/2 inch outside diameter tube employed in this system was constructed from fiberglass reinforced with a plastic resin by filament winding.

The instrumentation for measuring the charge gas properties during the compression process was contained in the thick flange at the end of the fiberglass tube.

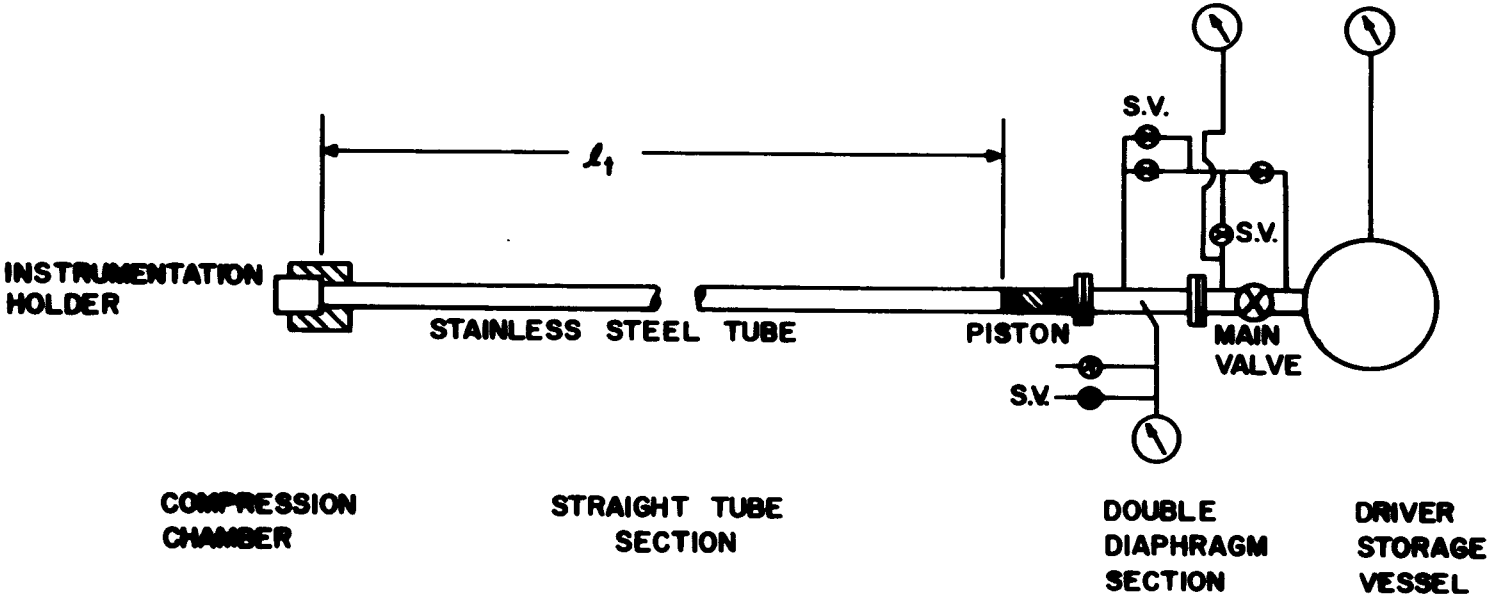

Figure 10 Schematic Diagram of 33 Atmosphere Piston System

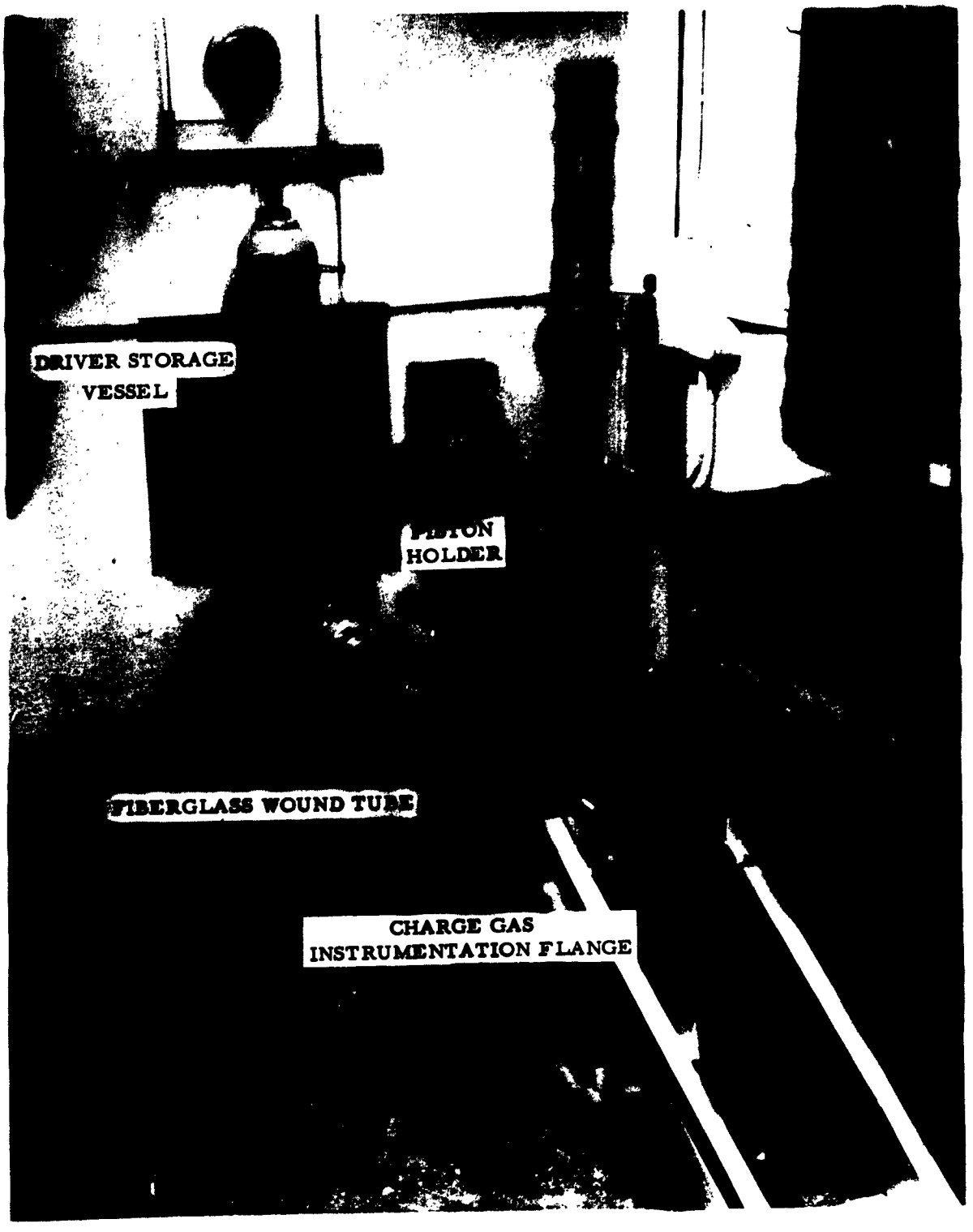

Figure 11 Photograph of 147 Atmosphere Piston System

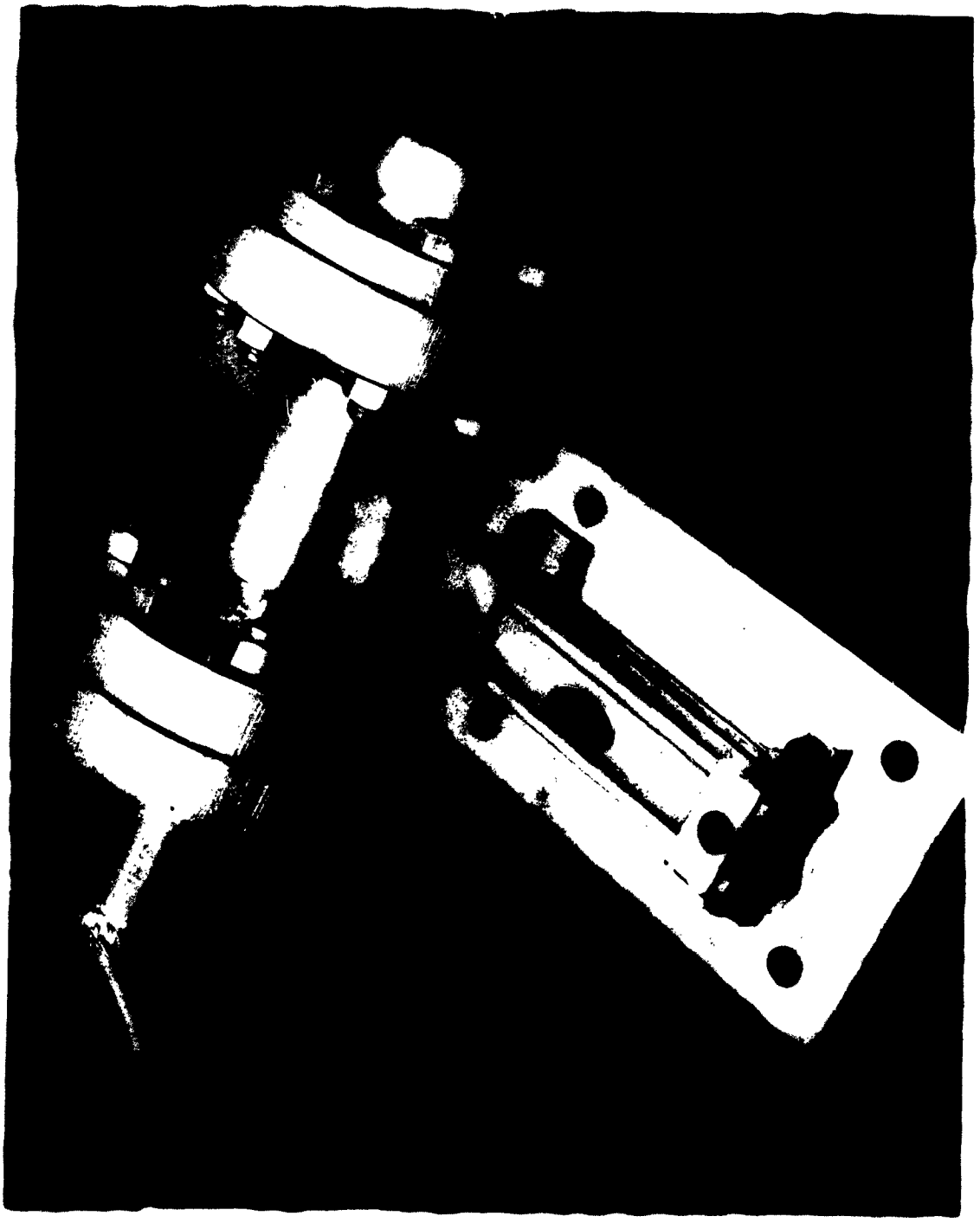

Figure 12 Photograph of Piston Holder of 147 Atmosphere Piston System.

Pressure measurements were obtained with Kistler 601 and 605 miniature pressure transducers used in conjunction with Kistler 655 or amplifiers. These transducers were mounted (with a Kistler 636 high adapter if required) at the closed end of the tubes and the pressure data played on the screen of a 551 dual beam Tektronix Oscilliscope where were photographed with a Polaroid Land Camera.

A butt-welded, 1 mil, chromel-alumel thermocouple was also i in the end flange of the 147 Atmosphere Piston System to obtain tempe time histories. The thermocouple output voltage was amplified by a K amplifier and was also recorded from the screen of the 551 Tektronix liscope.

In later tests the minimum volume was measured by a technique s that discussed in Reference 9. This technique utilizes a soft-metal pi tached either to the front of the piston or to the end of the tube, which formed on impact; the measurement of the length of the pin perpendicu the face of the piston after the test determines the minimum volume. leakage exists, the specific volume is known, and this in conjunction w peak pressure defines the thermodynamic state of the gas at the time o pressure. Measurements of the charge gas pressure, after the driver is released, along with the final piston position were utilized to determ leakage of the charge gas occurred during the compression process.

C. EXPERIMENTAL INVESTIGATIONS

1. 33 Atmosphere Piston System Tests

Three experimental test series were conducted with the 33 Atm Piston System utilizing air for both the charge and driver gases. The Probe Series was undertaken to evaluate the thermodynamic process a peak state of the charge gas for heavy piston operation of the free-pist pressor. To determine the effect of piston mass upon the free-piston pression process the Piston Mass Effect Series was conducted. In ord more firmly establish that the peak charge gas pressure ratio, π_m, fo heavy piston case is only a function of the driver pressure ratio and fr meters, and to extend the range of data obtained in the Volume Probe S Variable Charge Pressure Series was also conducted.

A fourth test series utilizing helium for the charge gas, the He Charge Series, was also conducted. This series was undertaken in an to varify the heavy piston theory for a charge gas other than air.

Tests to determine the static coefficient of friction for the pist rings indicated an average value of about 0.7. Since a value of 50% or of the static coefficient would not be unreasonable for the kinetic coeffi of friction a value of 0.3 was assumed for the kinetic coefficient of fric The residual friction force given by

$$f_R = (8c \frac{d}{D} \frac{S}{P_o}) (P_o A_p)$$

was evaluated both analytically and empirically. To determine this force analytically, considerations of the physical and mechanical properties of the O-ring material were applied to estimate the residual O-ring stress, S. The empirical determination consisted of pulling, at various rates, the piston through the compression tube with a cord attached to a spring scale. A value of 12.5 lb_f for f_R was found to agree reasonably well with both the calculations and the pulling tests.

For the Volume Probe Series, a heavy aluminum piston (piston No. 1 Table II) was machined to receive a soft wire probe in its face. Soft lead solder wire was used to construct the probes.

Measurements of the pressure and volume of the charge air in the compression tube after each test indicated that very little or no leakage occurred in most of the tests conducted with the 33 Atmosphere Piston System.

The results of the Volume Probe Series are shown in Figure 13, a plot of the peak charge gas pressure ratio versus the minimum volume ratio. Also shown in this figure is the line representing a polytropic exponent, n, of 1.31 which can be seen to agree quite favorably with the data.

Assuming that the charge gas behaves as a perfect gas throughout the compression process, the peak temperature ratio is simply the product of π_m and λ_m. The maximum charge temperatures, determined in this manner for the Volume Probe Series, are presented as a function of the effective driver pressure ratio in Figure 14. Also shown is the theoretical temperature ratio determined from Eq (14) utilizing a polytropic exponent of 1.31.

Five aluminum O-ring sealed pistons, each of different mass, were constructed and tested in the Piston Mass Effect Series. The mass, weight parameter $\gamma W_p/W$, and description of these pistons are listed in Table II.

TABLE II

Piston Data for 33 Atmosphere Piston System

Piston Designation	Mass (lb_m)	$\gamma W_p/W$ (air charge gas)	Description
1	0.305	127.2	Solid Aluminum, 4 in. long
2	0.148	62.7	Solid Aluminum, 2 in. long
3	0.116	48.4	Hollow Aluminum, 2 in. long
4	0.073	30.4	Solid Aluminum, 1 in. long
5	0.053	22.1	Hollow Aluminum, 1 in. long

($c = 0.3$, $f_R = 12.5\ lb_f$, $d = 0.103$ in., $D = 1$ in., $P_o = 14.4$ psia)

The data obtained at four representative driver pressure ratios in the piston Mass Effect Series is compared to the theoretical prediction curves in Figure 15, which is a plot of the peak charge air pressure ratio versus piston mass parameter $\gamma W_p/W$. The analytical heavy piston curves were obtained from Eqs (12) and (13) utilizing a polytropic exponent of 1.31 and the values of the other parameters listed at the bottom of Table II. The light piston theoretical curves were calculated as is described in Section II A-3 utilizing a

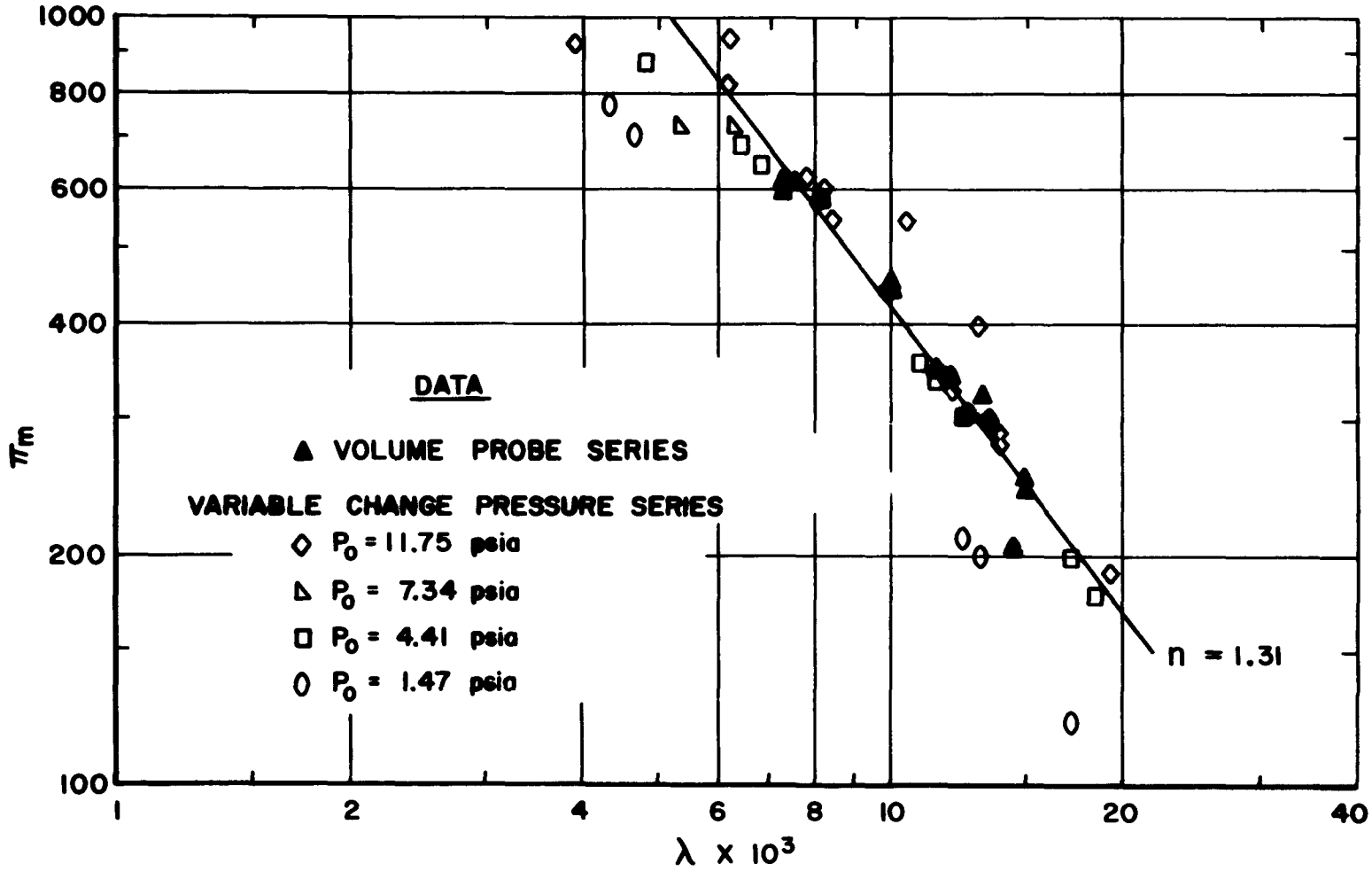

Figure 13 Peak Charge Air Pressure Ratio Data Versus Minimum Volume Ratio Data from the Volume Probe Series and Variable Charge Pressure Series (Heavy Piston).

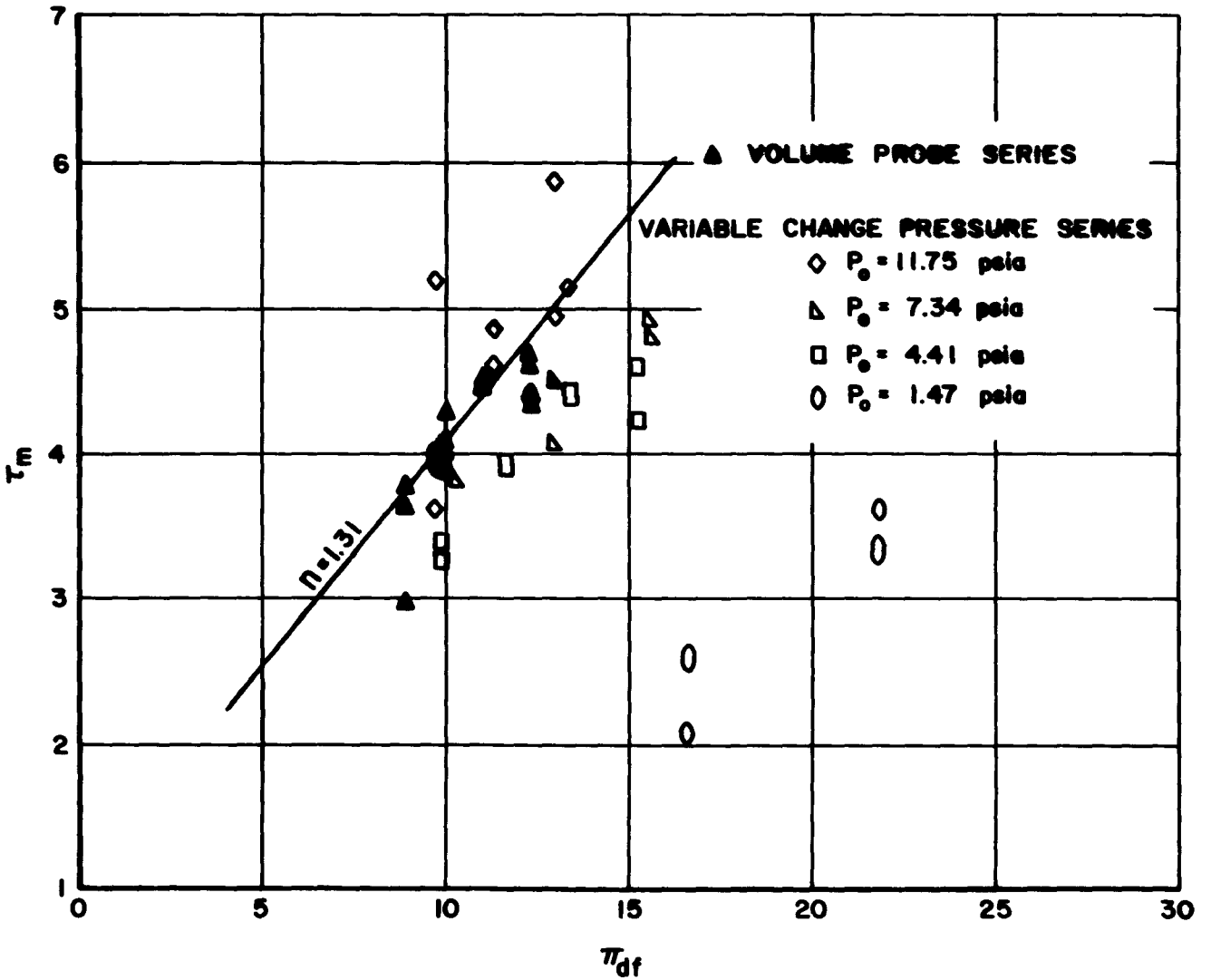

Figure 14 Comparison of Theoretical Temperature Ratio with Values Calculated from Experimental Data from the Volume Probe Series and Variable Charge Pressure Series (Heavy Piston).

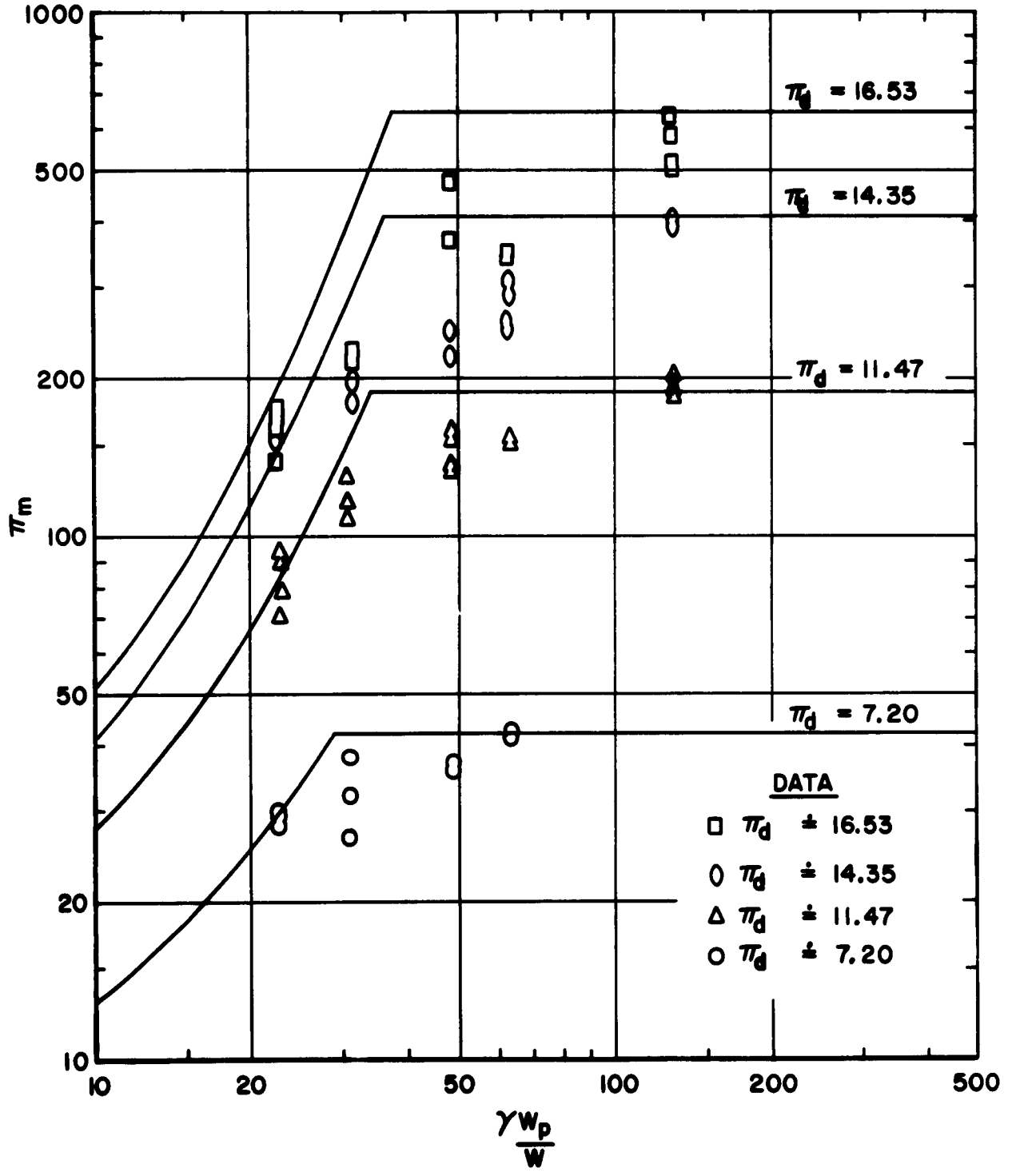

Figure 15 Comparison of Piston Mass Effect Data with Theoretical Peak Charge Air Pressure Ratio Predictions for 33 Atmosphere Piston System.

non-steady expansion of the driver air. The heaviest piston data agrees quite well with the heavy piston theory and the trend of the lighter piston data appears to fair into the light piston theoretical curves reasonably well. There is, however, a transition zone, as would be expected, in which neither theory is appropriate. This zone, although only a narrow range of $\gamma W_p/W$ for low values of π_d, increases with increasing driver pressure ratio. Also, it is noted that the deviation from the theoretical predictions within this zone, although small at the lower values of driver pressure ratio, becomes greater with increasing π_d.

To demonstrate the effect of friction upon the performance of the free-piston compression process the heavy piston theory, with and without friction, is presented in Figure 16 along with the heavy piston data (piston 1) obtained in the two test series discussed above.

The Variable Charge Pressure Series was conducted, as was the Volume Probe Series, employing a heavy aluminum piston (piston No. 1 Table II) and volume probes made of soft lead-solder wire. During these tests four different values of the initial charge air Pressure, which are listed in Table III were investigated at various driver pressure ratios to expand the range of data given in Figure 16 and also to more firmly establish that the peak charge pressure ratio, for the heavy piston case, is only a function of driver pressure ratio and friction parameters.

TABLE III

Initial Charge Air Pressure and Piston

Weight Parameter Data for Variable Charge Pressure Series

Initial Charge Pressure P_{1c}		$\gamma W_p/W$
atm.	psia.	
0.8	11.75	155.8
0.5	7.34	249.6
0.3	4.41	415.4
0.1	1.47	1247.7

($c = 0.3$, $f_R = 12.5$ lb$_f$, $d = 0.103$ in., $D = 1$ in., $P_o = P_{1c}$)

The results of the Variable Charge Pressure Series are compared to the results of the Volume Probe Series in Figures 13 and 14, and the peak charge air pressure ratio data is plotted as a function of the effective driver pressure ratio in Figure 17. The effective driver pressure ratios for these tests were calculated using Eq (11) utilizing the data given in Table III.

The peak pressure ratio data versus minimum volume ratio data agrees quite well with the previous results and theory, except for the data obtained at the lowest values of initial charge air pressure. A polytropic exponent of about 1.2 is indicated by this data which is considerably lower than 1.31 which agrees quite well with the data obtained for the tests conducted at the higher values of initial charge pressure. As shown by Figures 14 and 17 the peak temperature ratio and peak pressure ratio, for the data obtained for an initial charge

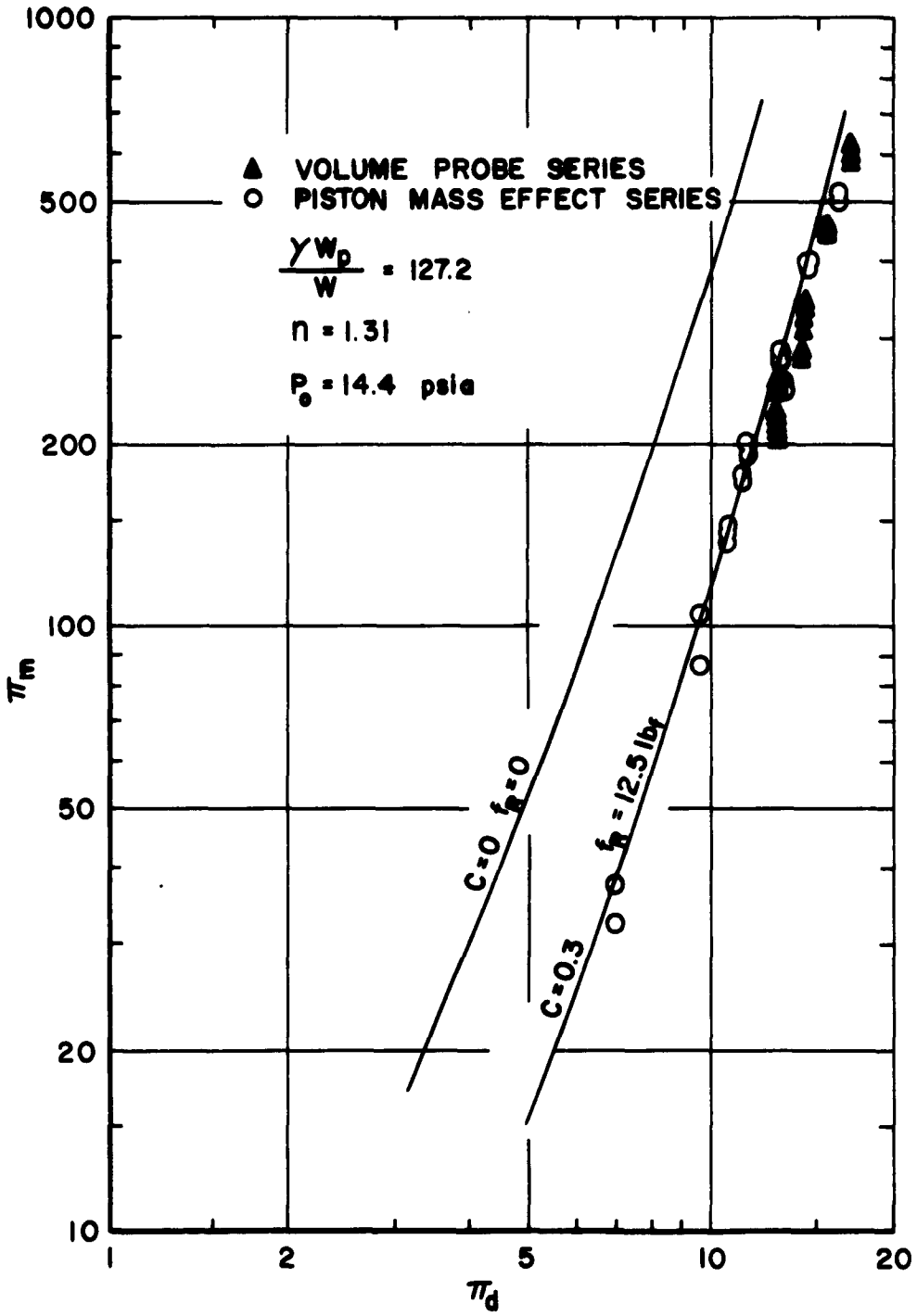

Figure 16 Comparison of Theoretical Peak Pressure Ratio and Experimental Data for 33 Atmosphere Piston System with Heavy Piston.

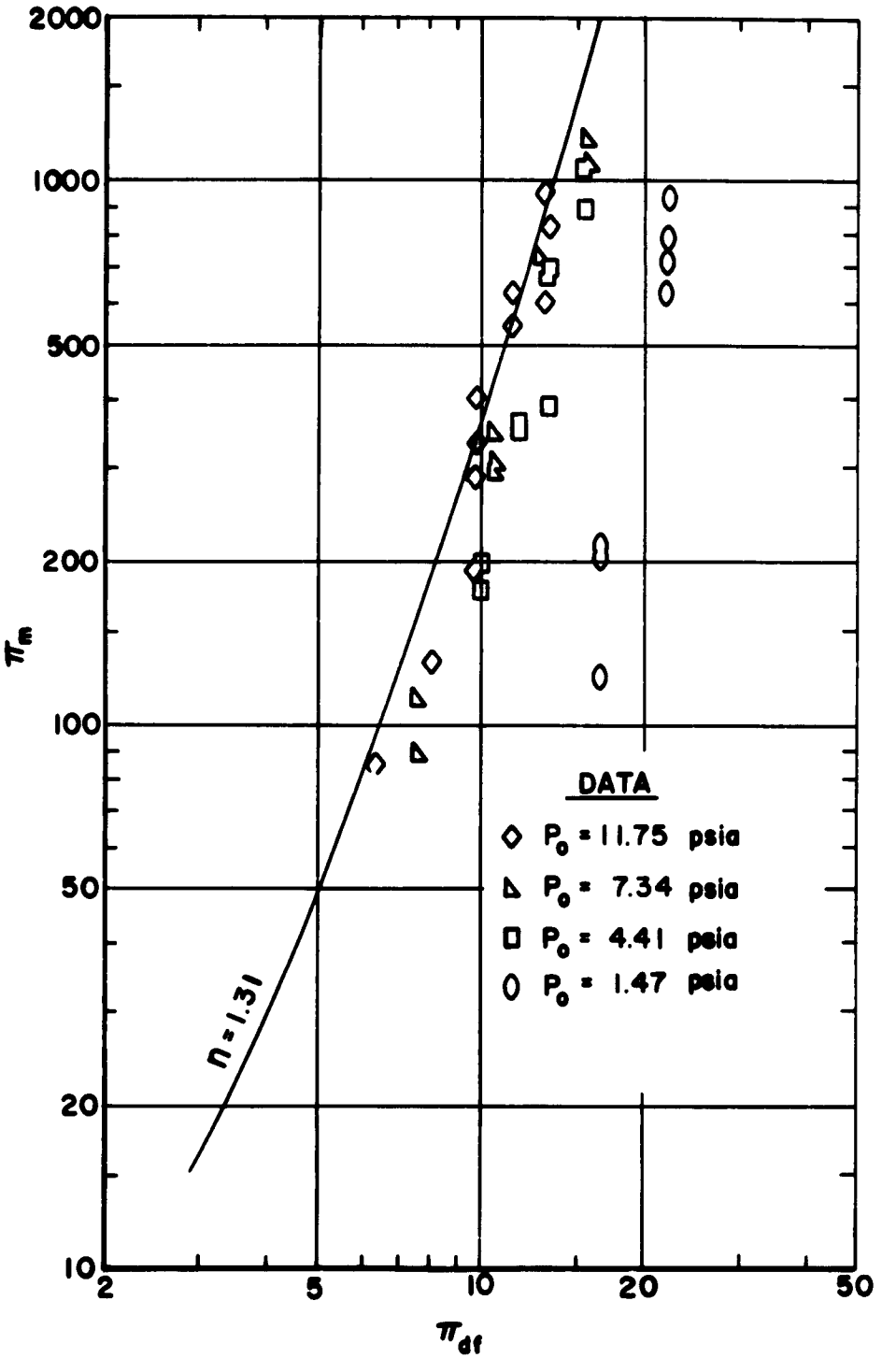

Figure 17 Comparison of Theoretical Peak Charge Air Pressure and Experimental Data from the Variable Charge Pressure Series.

air pressure of 0.1 atmosphere, are considerably lower than predicted by the heavy piston theory. This deviation, from the theoretical predictions, may in part be due to the fact that the residual friction alone represents 26% of the piston driving force at the highest value of driver pressure employed for this series. Thus any actual deviation from the assumed friction parameters would yield considerable deviation from the predicted performance. Also in view of the relatively low driving force, the compression time is considerably longer, thus, the heat losses more severely degrade the performance at these low values of initial charge air pressure.

The Helium Charge Series, in which helium was employed for the charge gas and air as the driver gas, was undertaken in an attempt to verify the heavy piston theory for a charge gas other than air. Again the heaviest aluminum piston with volume probes was employed. It was, however, necessary during this series to substitute soft aluminum for the lead-solder wire for construction of volume probes. The temperatures obtained during these tests were great enough to melt the lead-solder probes.

The results of this test series are presented in Figures 18, 19, and 20. The peak charge gas pressure ratio data, plotted as a function of minimum volume ratio in Figure 18, show good agreement with the theoretical predictions obtained using a polytropic process with a polytropic exponent of 1.50. However, the maximum temperature ratio and peak pressure ratio data, presented as a function of effective driver pressure ratio in Figures 19 and 20 respectively, indicate that the performance is less than theoretically predicted at higher values of the effective driver pressure ratio. One plausible explanation for this trend is that Eq (11) does not sufficiently correct the driver pressure ratio for frictional effects at higher values of the driver pressure ratio. This may be due to the fact that the friction parameters are considered constant. Therefore, an investigation as to their dependence upon driver pressure ratio and velocity may yield data which would allow more accurate predictions utilizing the present theory.

2. 147 Atmosphere Piston System Tests

Three O-ring sealed pistons, each of different mass, were constructed and tested with the 147 Atmosphere Piston System. The mass, weight parameter $\gamma W_p/W$, and description of these pistons are tabulated in Table IV.

TABLE IV

147 Atmosphere Piston System Piston Data

Piston Designation	Mass (lb_m)	$\gamma W_p/W$ (air charge gas)	Description
a	0.132	348	Steel, 2.86 in. long
b	0.066	175	Steel, 1.64 in. long
c	0.028	74	Aluminum, 1.73 in. long

($c = 0.2$, $f_R = 5\ lb_f$, $d = 0.070$ in., $D = 1/2$ in., $P_o \doteq 14.4$ psia)

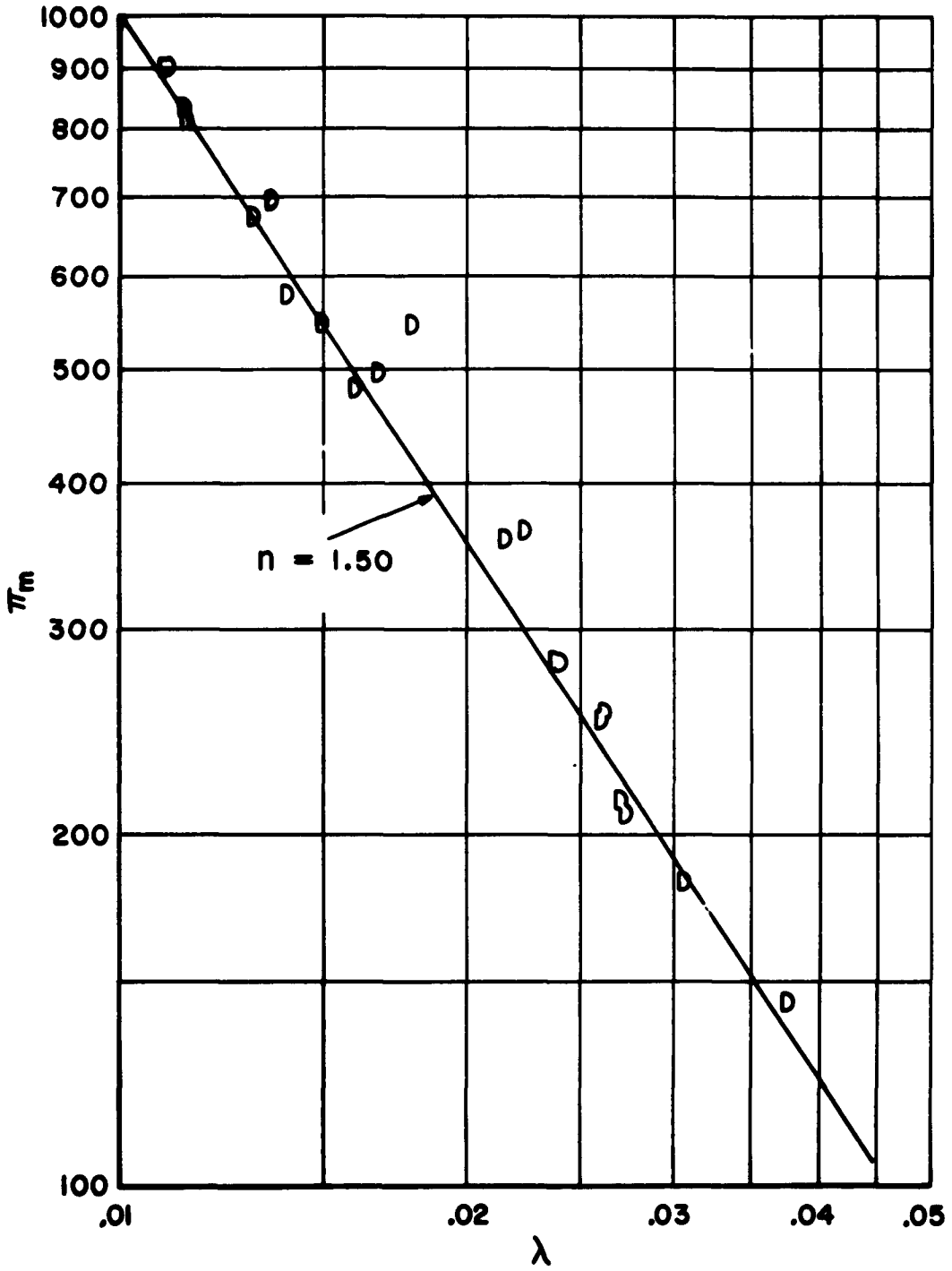

Figure 18 Peak Charge Gas Pressure Ratio Data Versus Minimum Volume Ratio Data from the Helium Charge Series.

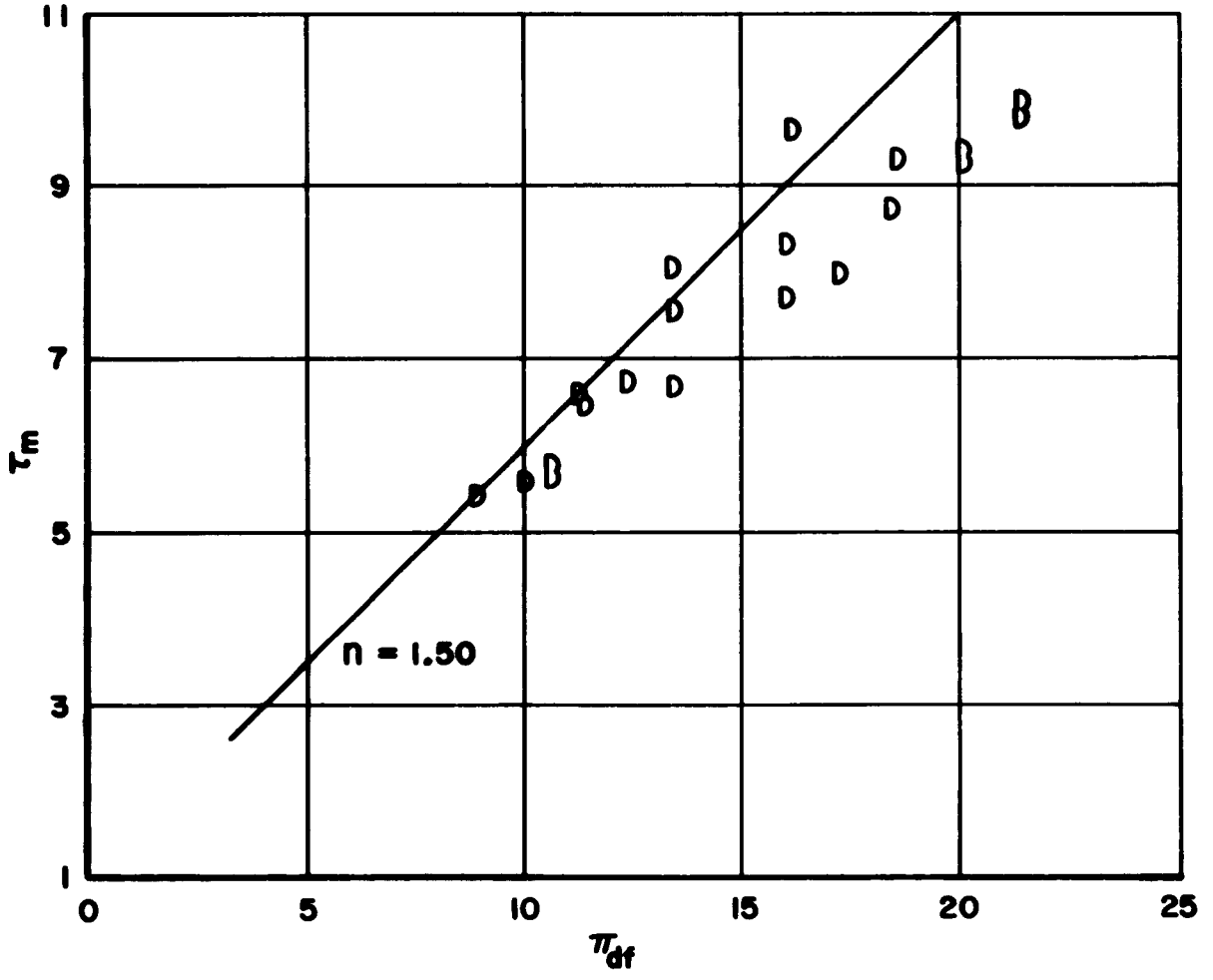

Figure 19 Peak Helium Temperature Ratio Calculated from Esperimental Data from the Helium Charge Series Compared with Theoretical Heavy Piston Predictions.

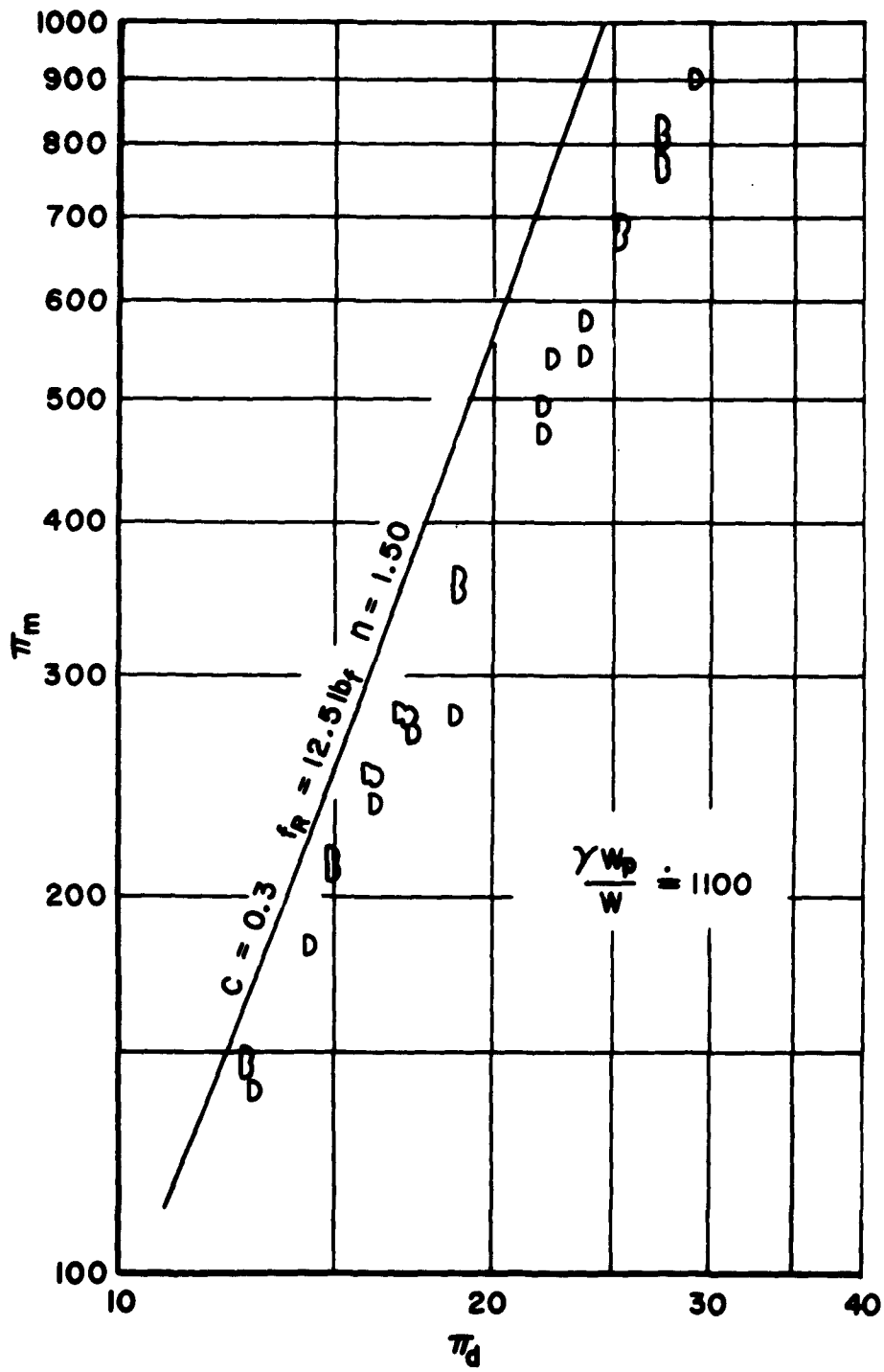

Figure 20 **Peak Theoretical Helium Pressure Ratio and Experimental Helium Peak Pressure Ratio Versus Driver Pressure Ratio.**

The relative sizes of the heavy steel (piston a) and aluminum piston (piston c) are shown in Figure 21. The lighter steel piston (piston b) is geometrically identical to the aluminum piston. Figure 22 is a photograph of a disassembled aluminum piston. The construction of both steel pistons is identical to the aluminum piston except for the longer end caps on the heavy steel piston.

The Teflon rings shown in Figures 21 and 22 are of slightly larger diameter than the piston body. They serve both as back-up rings for the O-ring seals and as guides which aid in aligning the accelerating piston in the straight tube. The large groove in the center of the pistons is provided for engagement with the piston holder plunger.

A value of 0.2 for the kinetic coefficient of friction for the piston O-rings on the reinforced fiberglass wound compression tube was found to correlate well with the test data. A value of 5 lb_f for the residual piston friction force was found to agree reasonably well with both the analytical calculations and the pulling tests performed with this system.

In addition to the miniature quartz pressure transducer, 1 mil cromel-alumel thermocouples were installed in the end flange to obtain temperature histories of the charge air. Although, the response time of these thermocouples was insufficient to adequately follow the charge air temperature, an extrapolation technique was employed in an attempt to determine the peak charge air temperature. This procedure consisted of accepting the indicated temperature as correct at the time the temperature-time slope is zero. Utilizing this temperature and the corresponding pressure, a polytropic process was fitted between this state and the initial charge air state to determine a value for n. The maximum temperature was then calculated using the peak pressure with this value of n. The maximum temperature, obtained by this technique, is known to be less than the actual value since it would be necessary for heat to be added during the charge air expansion for the entire process to be polytropic with a constant value of the exponent n. The maximum temperature ratio data, obtained in this manner for the 147 Atmosphere Piston System tests, is presented in Figure 23.

The maximum charge air pressure ratio data is compared to the heavy piston theory, with and without friction, in Figure 24. A value of 1.31 was applied to the theory for the polytropic exponent n.

A volume probe test series was undertaken with the 147 Atmosphere Piston System but was abandoned when leakage of the charge air could not be prevented.

D. CONCLUSIONS

Figures 16 and 24 serve to clearly demonstrate the degradation of performance of the ballistic-piston compression process due to piston frictional effects and the good agreement between the data and heavy piston theory.

Although data at lower values of the piston mass parameter may be desirable to more precisely evaluate the light piston theory, the present data and theories do qualitatively establish the effect of piston mass upon the

HEAVY STEEL PISTON

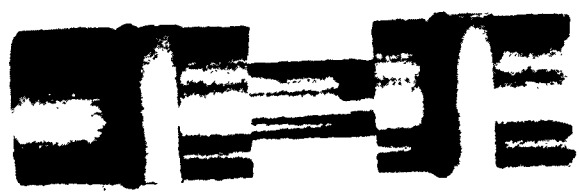

ALUMINUM PISTON

Figure 21 Photograph of the Aluminum and Larger Steel Pistons for the 147 Atmosphere Piston System.

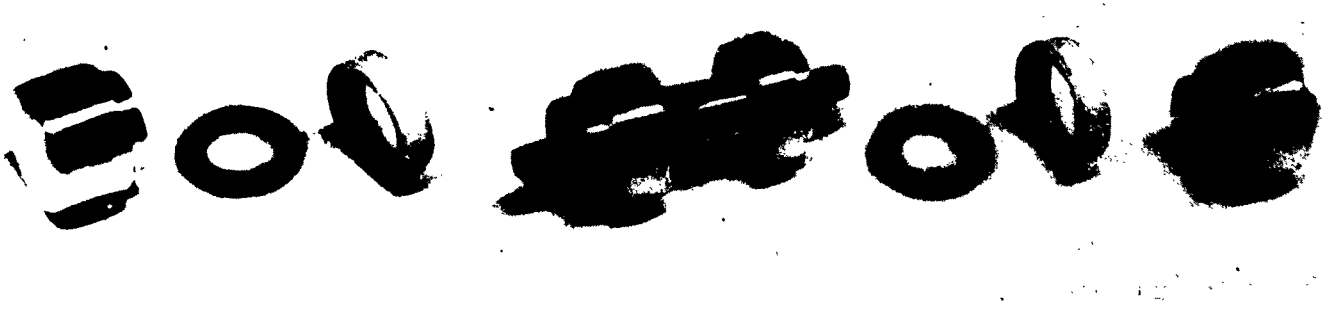

Figure 22 Photograph of Disassembled Aluminum Piston for 147 Atmosphere Piston System.

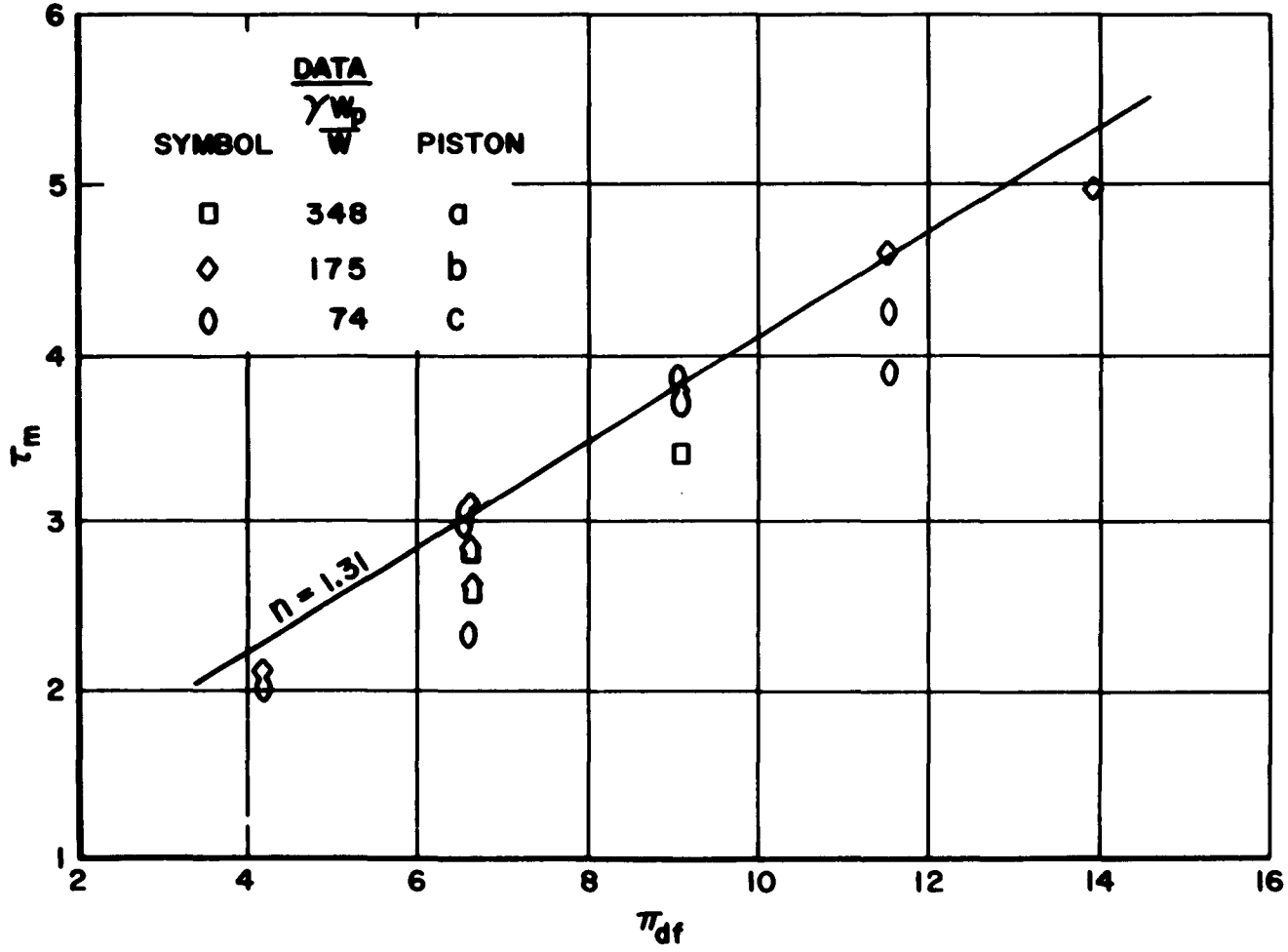

Figure 23 Peak Charge Air Temperature Ratio Extrapolated from Experimental Data from the 147 Atmosphere Piston System Compared with the Theoretical Heavy Piston Prediction.

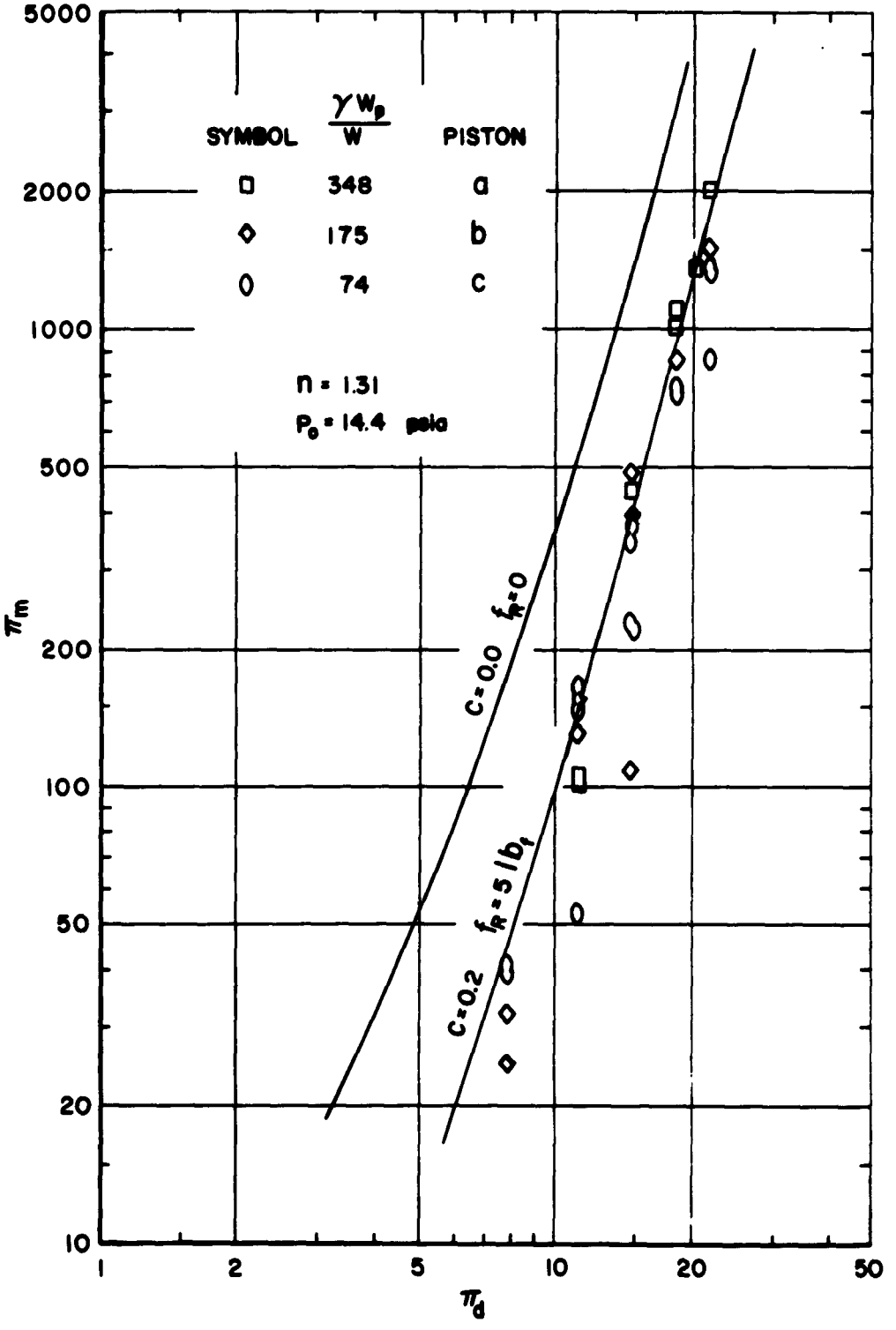

Figure 24 Comparison of Theoretical Peak Pressure Ratio and Experimental Data for 147 Atmosphere Piston System with Heavy Piston.

performance of the free-piston compressor. The data clearly indicates that the performance of the heavy piston case is independent of piston mass, whereas for the light piston case the piston mass is truly a significant variable.

To allow more accurate theoretical predictions of the free-piston compression process at higher values of the effective driver pressure ratio, it may be desirable to determine the friction parameters, both residual friction and kinetic coefficient of friction, as a function of driver pressure ratio and piston velocity rather than use constant values for these parameters as was done for the present studies.

SECTION III

LIQUID-DRIVEN PISTON COMPRESSION PROCESS

The liquid-driven piston compressor was contrived to investigate the performance characteristics of a system which utilizes the kinetic energy of a liquid column to compress the charge gas. The function of the piston is primarily to maintain separation of the liquid column and the charge gas.

The schematic diagram of the liquid-driven piston compressor is essentially the same as that for the free-piston compressor given in Figure 1. The driver liquid, initially stored in the driver storage vessel, is accelerated, upon release of the piston, by a high pressure air cushion above the driver fluid in the storage tank. This high-speed column is in turn decelerated by the charge gas initially occupying the volume of the straight tube.

A theoretical investigation of the liquid to gas compression process is presented in Section III of Reference 1. This study, which assumes the piston physical properties to be identical to those of the driver liquid, yielded analytical relations for the peak charge gas pressure ratio obtained in the charge air for a given set of conditions: polytropic compression process, strain energy storage distribution in the liquid column, coefficient of friction, and geometry. The first solution of the momentum equation was based upon the assumption of incompressible flow, however, later modifications included strain energy storage in the driver liquid column.

Three relations for the peak charge gas pressure ratio were presented in Reference 1. The first neglected strain energy storage in the driver liquid. The second assumed strain energy to be stored in the driver liquid with a linear pressure gradient from the gas pressure at the liquid-gas interface to driver pressure at the tank outlet. The third considered the strain energy to be stored in the liquid column at constant pressure equal to the charge gas pressure. Since the first two of these relations yielded peak pressures greater than the water hammer pressure, a solution, which considered compressibility effects in both the liquid and gas, was accomplished on a digital computer to gain further insight into the occurring phenomena. This development is presented as follows.

A. THEORETICAL CONSIDERATIONS

The simplified liquid model, which was assumed for this study, consisted of a semi-infinite straight tube containing a liquid column at uniform velocity which impinged on a closed end air column initially at atmospheric conditions. The compression was assumed to be adiabatic and frictional effects were neglected. Upon impact with the air column compression waves would be transmitted into both the liquid and the gas, and the boundary conditions at the interface required that the liquid pressure equal the gas pressure and that the liquid velocity equal the gas velocity. The wave phenomena in both the liquid and gas were followed until the interface stopped.

The relation between velocity and pressure across a wave in the liquid is:

$$P_y = P_x + \rho_\ell s(u_x - u_y). \tag{28}$$

The equation in the gas is:

$$P_y = P_{xr}\left[\frac{2\gamma}{\gamma+1}\left(\frac{c_y}{a_{xr}}\right)^2 - \frac{\gamma-1}{\gamma+1}\right] \tag{29}$$

and $\frac{c_y}{a_{xr}}$ is given by

$$\frac{c_y}{a_{xr}} = \frac{\gamma+1}{4}\frac{u_y}{a_{xr}} + \frac{1}{2}\sqrt{\left(\frac{\gamma+1}{2}\frac{u_y}{a_{xr}}\right)^2 + 4}. \tag{30}$$

The shock in the gas impinges on the wall and is reflected towards the interface, and the boundary condition at the wall requires that the gas velocity be zero.

The equations are:

$$\frac{P_{yr}}{P_y} = \frac{2\gamma}{\gamma+1}\left(\frac{u_y + c_{yr}}{a_y}\right) - \frac{\gamma-1}{\gamma+1}, \tag{31}$$

where

$$\frac{u_y + c_{yr}}{a_y} = \frac{\gamma+1}{4}\frac{u_y}{a_y} + \frac{1}{2}\sqrt{\left(\frac{\gamma+1}{2}\frac{u_y}{a_y}\right)^2 + 4}. \tag{32}$$

Equations (28) through (32), equations for other gas properties, and the equation for the time required for waves to travel between the interface and wall were appropriately normalized and programmed for a digital computer. Equations (28), (29) and (30) were solved by an iteration procedure to satisfy the boundary conditions at the interface. The normalization of the equations yielded $\rho_\ell s a_o / P_o$, γ and u_o/a_o as the significant dimensionless parameters in the study where u_o is the initial liquid column velocity.

The peak values of the data obtained are shown in Table V. The value of $\rho_\ell s\, a_o/P_o$ which was used would be correct for water as the driver fluid and air, at atmospheric conditions, as the charge gas.

TABLE V

$$\rho_\ell s\, a_o/P_o = 4808.0 \quad \gamma = 1.4$$

u_o/a_o	π_m	τ_m	λ_{min}	t'	Approx. π_d	Approx. π_{wh}	Approx. t'	$\tau = \pi^{\frac{\gamma-1}{\gamma}}$
0.15	722	6.58	0.00911	7.09	13.0	721	7.00	6.55
0.20	962	7.16	0.00744	5.26	23.1	962	5.25	7.12
0.25	1203	7.66	0.00637	4.19	36.2	1202	4.20	7.61

The approximate value of π_d was determined from steady flow considerations:

$$\frac{1}{2}\ \rho_\ell u_o^2 \doteq P_d$$

and therefore,

$$\pi_d \doteq \frac{\gamma}{2}\ \frac{\rho_\ell}{\rho_o}\left(\frac{u_o}{a_o}\right)^2 \quad . \tag{33}$$

The approximate value of the water hammer pressure, π_{wh}, was determined as follows:

$$P_{wh} = \rho_\ell\ s\ u_o$$

hence

$$\pi_{wh} = \frac{\rho_\ell s\, a_o}{P_o}\left(\frac{u_o}{a_o}\right). \tag{34}$$

The time for the compression process will be approximately given by

$$t \doteq \frac{\ell_c}{u_o}$$

or

$$t' \doteq \frac{a_o}{u_o} \quad .$$

A better approximation, however, over the range of velocities studied is

$$t' \doteq 1.05 \frac{a_o}{u_o} . \tag{35}$$

The last column in Table V indicates that the reversible adiabatic compression yields a reasonable value for the temperature ratio. This would be valid until high subsonic values of u_o/a_o are obtained.

In the solution of the problem it was assumed that a semi-infinite tube contained the original liquid column, however, a finite tube would be sufficient if the compression process was completed before the first reflected wave returned in the liquid to the interface. Hence if

$$\left(\frac{2\ell_t}{s}\right) \frac{a_o}{\ell_c} \geq t' \tag{36}$$

or

$$\frac{\ell_t}{\ell_c} \geq \frac{1}{2} \frac{s}{a_o} t' \tag{36}$$

the compression process would be completed before the reflected wave from the driver tank returned to the interface. Combining Eqs (35) and (36) we have

$$\frac{\ell_t}{\ell_c} \geq 0.525 \frac{s}{a_o} \frac{a_o}{u_o} \tag{37}$$

For water and air at atmospheric conditions we have

$$\frac{\ell_t}{\ell_c} \geq 2.23 \frac{a_o}{u_o} .$$

For u_o/a_o of 0.25 a 1 foot long charge of air at atmospheric conditions could be compressed in a tube approximately 10 feet long; for $u_o/a_o = 0.15$ a tube of 16 feet would be sufficient to compress a 1 foot charge of air.

The data from the program, which considered compressibility effects, indicated that the water hammer pressure is the maximum pressure which can be achieved from a liquid-air system.

B. EXPERIMENTAL INVESTIGATIONS

Tests, utilizing the liquid driven piston compression concept, were conducted with the 147 Atmosphere Piston System which was described in the preceding section. All three pistons, described in Table IV, were used in these tests in which water was employed as the driver fluid and high pressure air, stored above it in the tank, as the working fluid.

The charge gas pressure history was recorded for these tests in the same manner as was described for the free-piston compression process. The peak pressure ratio data are plotted as a function of driver pressure ratio, for all three pistons, in Figure 25. Ambient air was used for the charge gas for all tests.

The data of Figure 25, indicate that the performance, and thus the peak charge gas pressure, is dependent upon piston material and length as well as driver pressure. Also, it is important to note that peak charge gas pressures, in excess of water hammer or water impact pressure, have been obtained in these tests. It is felt that this effect is due to the ability of the piston to withstand a significant pressure gradient and not due to any phenomena in the liquid.

C. CONCLUSIONS

The liquid driven piston data, Figure 25, clearly demonstrate that pressures in excess of water hammer have been achieved experimentally. A result which is even more significant since the velocity used to calculate the water hammer pressure was obtained neglecting the effects of friction. The experimental results demonstrate that the piston permits higher pressures than water hammer to be obtained. In fact the maximum pressure obtainable (an upper limit which cannot actually be achieved) would appear to be the impact pressure (a stress which is analogous to water hammer) which is determined from the properties of the piston material and the velocity. Hence, it is seen that the piston, besides separating the two fluids, enables higher pressures to be achieved than the impact pressure in the driver fluid.

The theory based upon a constant pressure in the liquid column, equal to the pressure at the liquid-gas interface, would represent the process if no piston were present. However, since this analysis, based upon conservation of momentum and energy, does not take into account the presence of the piston, it does not adequately define the phenomena for a liquid driven piston system. Therefore, no attempt to compare the test results with the previously developed theories was undertaken.

SECTION IV

STAGED PISTON-COMPRESSION SYSTEMS

During the past year engineering efforts were also directed towards the development of a high pressure staged piston system designated as the Tandem Staged Piston System. The tandem system utilizes the main driver supply of liquid or gas to produce a high pressure driver fluid for the second stage. In the second stage the charge gas is compressed to a high density and temperature.

A preliminary theoretical study was accomplished for a staged system designated as the Parallel Staged Piston System. The parallel system utilizes two stages to compress and recompress the charge gas with a free expansion between stages.

The design of the Tandem Staged Piston System has been completed and this system is presently under construction.

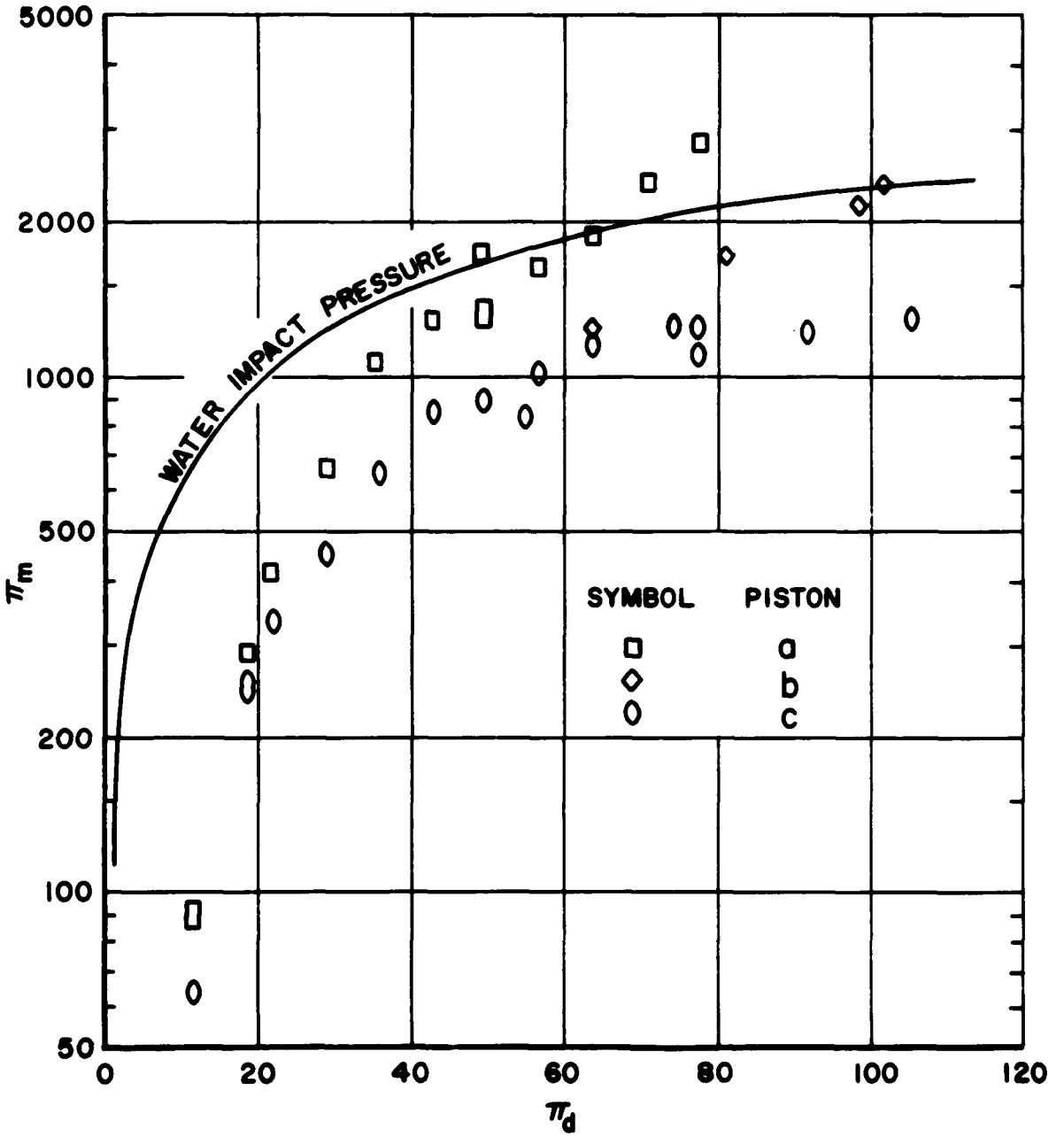

Figure 25 Peak Charge Air Pressure Ratio Data Versus Driver Pressure Ratio for Water Driven Piston Tests with 147 Atmosphere Piston System.

A. TANDEM STAGED PISTON SYSTEM

The tandem staged system is believed to be a device capable of producing very high density and high temperature gases, best suited for small quantities of charge gas for use in gas property investigations. The purpose of the present investigation is to determine this feasibility.

1. Conception

The first stage tube and main driver fluid supply of the tandem staged system are utilized to produce a high pressure or high temperature and pressure driver supply for the second stage. The charge gas is compressed in the coaxial second stage cylinder which is of relatively small diameter and length when compared to the first stage. Figure 26 depicts schematically the two configurations of this system which are planned for testing.

a. Liquid Driven Configuration

In the first configuration, shown in Figure 26A, the first stage cylinder is initially evacuated. Upon release, the liquid driven piston is allowed unrestricted travel throughout the length of the first stage; frictional effects having been ignored. A high pressure air cushion above the liquid driver supply, in the main driver reservoir, will be utilized to accelerate the liquid driver column and the first stage piston. Upon completion of the stroke in the first stage, the piston will be abruptly decelerated producing a shock wave, at the piston-liquid interface, which travels upstream at approximately the speed of sound in the liquid. The pressure behind this wave is the impact pressure which is proportional to the arrested flow velocity and to the speed of propagation of the pressure wave. The liquid impact pressure will be sufficient to burst the first stage piston diaphragm and allow the very high pressure liquid to accelerate the second stage piston into the charge gas, compressing it to a very high density and high temperature. The time of the charge gas compression process must be less than the time required for the shock to travel to the main driver reservoir and an expansion wave to return to the piston.

Figure 27 is a plot of water impact pressure as a function of the main reservoir driver pressure; see Eq (47) of Reference 1. A main driver reservoir pressure of 62 atmospheres would produce a water impact pressure of 1900 atmospheres in the first stage cylinder. Data obtained from the 147 Atmosphere Piston System, utilizing a water driven piston, indicates that charge gas pressures in excess of water impact pressures can be realized. Thus, with a second stage water driver supply at 1900 atmospheres peak charge gas pressures of the order of 20,000 atmospheres should be readily obtained.

b. Gas Driven Configuration

The second configuration of the tandem staged system is depicted schematically in Figure 26B. In this configuration, the first stage piston is accelerated by a high pressure gas supply, initially stored in the main driver reservoir. A first stage charge gas is compressed to high pressures and temperatures as it decelerates the piston. This gas in turn bursts the second stage diaphragm and accelerates the second stage piston which compresses the charge gas stored in the second stage cylinder. Data already obtained

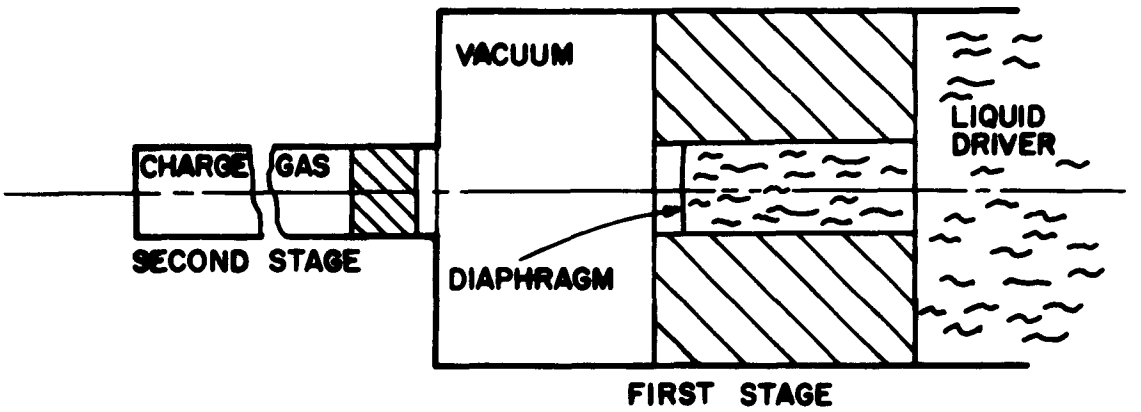

(A)

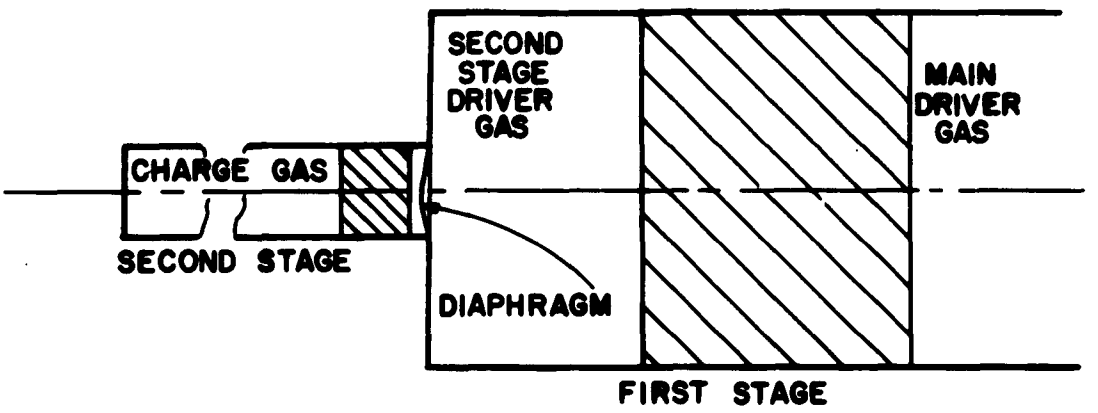

(B)

Figure 26 Schematic Diagrams of the Two Configurations of the Tandem Staged Piston System which Are Scheduled for Testing.

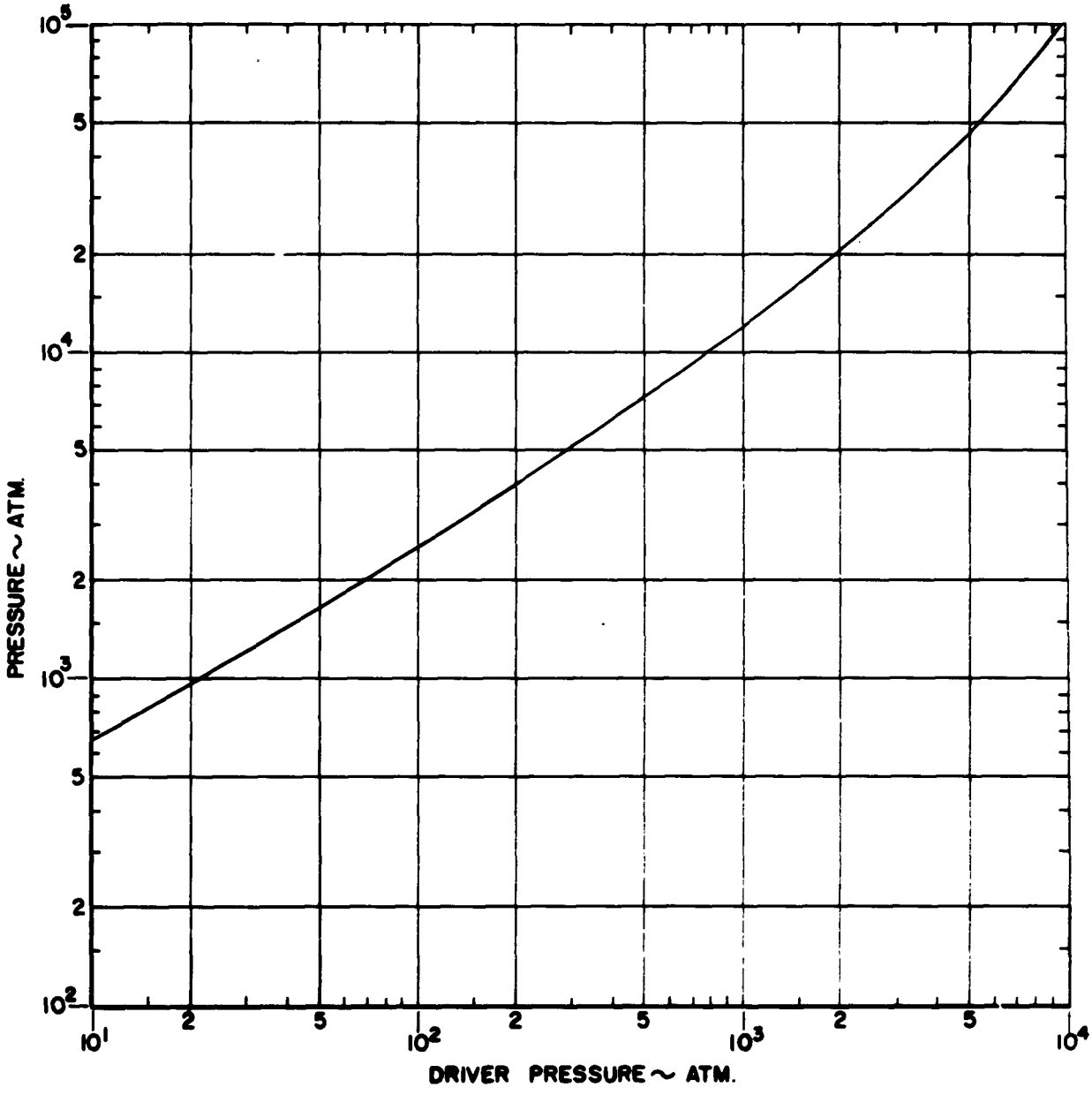

Figure 27 Water Impact Pressure. ("Water Hammer Pressure") Versus Driver Pressure.

indicates that very high second stage driver, first stage charge pressures, can be obtained with relatively low main driver pressures. However, the duration of the peak pressure is very short, thus the second stage diaphragm rupture must be synchronized to obtain the maximum amount of work from the second stage driver gas before its energy is expended in accelerating the first stage piston upstream. For this configuration it may also prove useful to conduct tests without the second stage piston. The second stage charge gas compression would then be accomplished through a number of shocks and a polytropic gas to gas compression.

2. Design

The design of the Tandem Staged Piston System (see Figure 28) has been completed and its construction is well underway.

A 6 cubic foot, 3000 psi, pressure vessel will be used as the main driver supply reservoir for the tandem staged system. The piston holder design is basically the same as that which proved successful for the 147 Atmosphere Piston System. The major change from the earlier design is that for this system the piston restraining plunger will restrain the piston at its face. This was deemed preferable to weakening the piston by machining a groove about its circumference, especially in view of the extreme loads which the piston must endure in this system. The static seal of the main reservoir driver fluid will be O-rings inserted in the wall of the piston holder. The seal of the driver fluid during the first stage compression (i.e. after piston release) will be accomplished by a Teflon sleeve around the first stage piston.

The 10 foot long first stage cylinder, of 2 inch inside diameter and 5 inch outside diameter, will be capable of withstanding pressures up to 45,000 psi. This stage is being constructed in two 5 feet lengths of Nationalloy No. 7 steel and to prevent corrosion will be chromium plated after machining. In each section of this stage, three special plugs will be inserted in the wall for instrumentation.

The second stage will be comprised of three one foot 0.388 inch inside diameter and 5 inch outside diameter cylindrical sections. Each section will consist of a two-layer shrunk fit composite cylinder in which the inner liner is to be constructed from Allegheny-Ludlum 18 percent nickel - 300 maraging steel and the outer layer from Nationalloy No. 7 high strength steel. The second stage tube will have an internal working pressure capability of 300,000 psi.

B. PARALLEL STAGED PISTON SYSTEM

The parallel staged system is believed to be a device capable of producing high density and high temperature gas in quantities sufficient for the operation of a hypersonic tunnel. The engineering time devoted to this system was directed towards the study of a model of sufficient size to determine the feasibility of the parallel staged system for application as the driver source for a hypersonic tunnel.

In the first stage of this system the charge gas, initially occupying the entire volume of the cylinder, is compressed by a gas driven piston to a high pressure and high temperature. This high energy density charge immediately

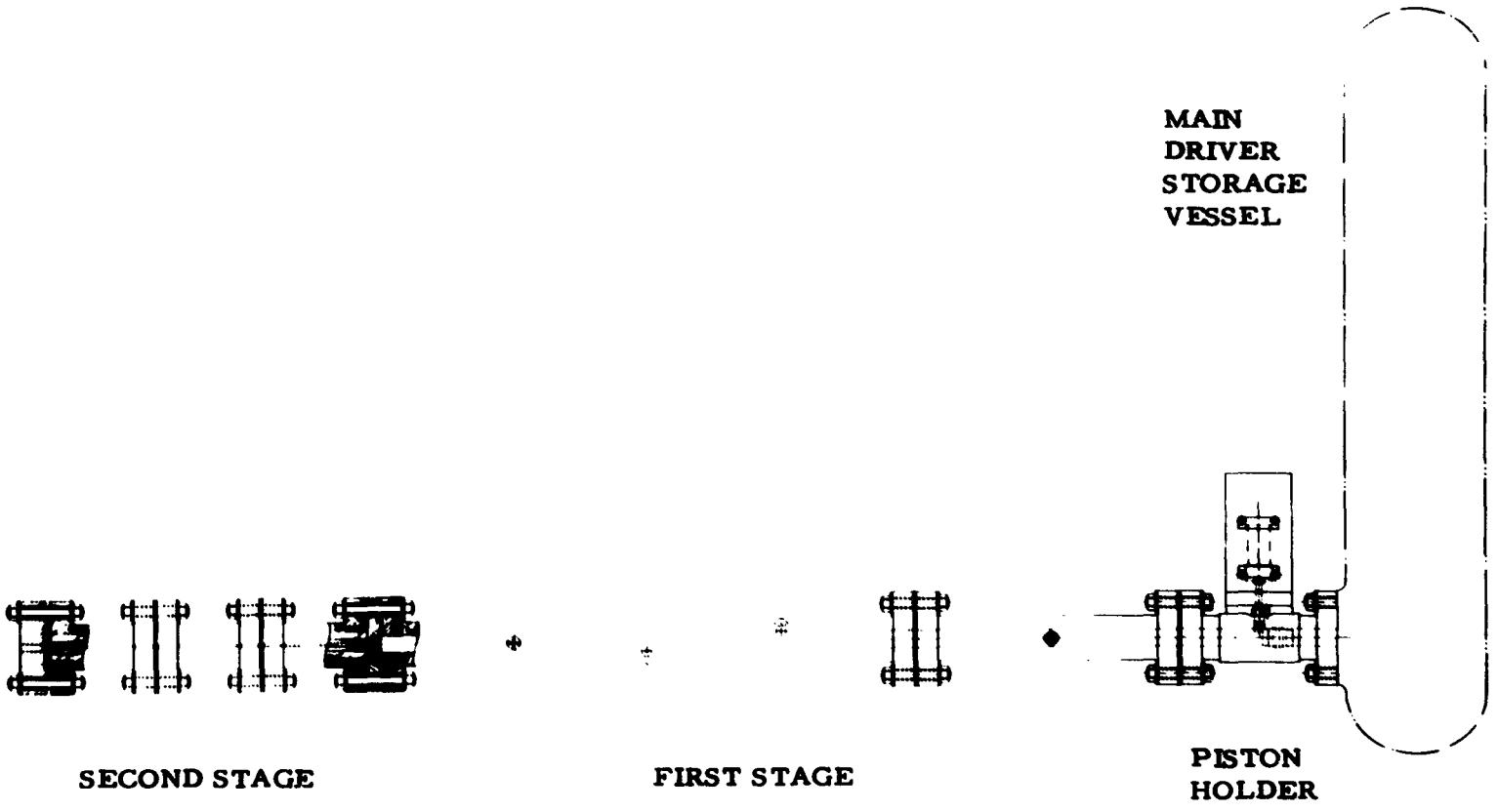

Figure 28 Physical Arrangement of Tandem Staged Piston System.

undergoes a free expansion into a second evacuated cylinder. In this second stage the charge gas is then recompressed by the second stage gas driven piston. At this point the charge gas could be expanded through a hypersonic nozzle into a tunnel.

Figure 29 is a chart of the thermodynamic properties of high temperature air. If standard sea level conditions are used for the initial charge air properties (point 1 in Figure 29) and the first stage compression to 3000 atm. is assumed to be isentropic, the final state of the charge air before expansion into the second stage is denoted as point 2. The state of the charge air in the second stage cylinder after a free expansion is dependent on the volume of the second stage. Theoretically the free expansion could yield any one of the states of increased entropy along the line of constant internal energy passing through point 2. Points 3, 4 and 5 representing second stage volumes of 1, 10 or 100 times the first stage volume, are indicated as plausible selections.

These initial conditions were selected since the second stage compression could then quite reasonably yield final temperatures in excess of 5550°K without requiring final pressures in excess of 3000 atm.

Utilizing the final expansion state indicated at point 3 might possibly yield a design in which the performance of the system would fall short of 5550°K due to energy losses in the form of heat and friction while that indicated at point 5 would require an excessively large second stage. Thus point 4 was selected as a compromise between these limits.

Assuming a second stage isentropic compression yields a final temperature of about 8300°K and pressure of 3000 atm, point 6 in Figure 29. It is of course realized that the above processes are ideal and that due to energy losses in the form of heat and friction the performance of the parallel staged system will be somewhat less than discussed above. However, it would be the purpose of an experimental investigation to determine the degree of degradation of performance due to losses and to determine if they can be reduced to levels which are tolerable for the successful operation of this system for use as the driver source for a hypersonic tunnel.

SECTION V

LIQUID-AIR INTERFACE STUDIES

Since in some applications the use of a piston for providing separation of the liquid driver and charge gas may not be desirable, the problem of maintaining a stable liquid interface arises for a liquid driven gas compression system. An investigation of tapered tubes which would accelerate the liquid driver for longer periods of time, and thus would delay interface break up, was reported in Reference 1. This investigation has been extended and is presented on the next page. Also presented is a solution for tailoring a tube to have a constant interface velocity.

An experimental program with a liquid driven system, utilizing membranes in tapered tube sections to maintain separation of the driver fluid and charge gas, has been more recently undertaken. The preliminary results of this program are described in following paragraphs.

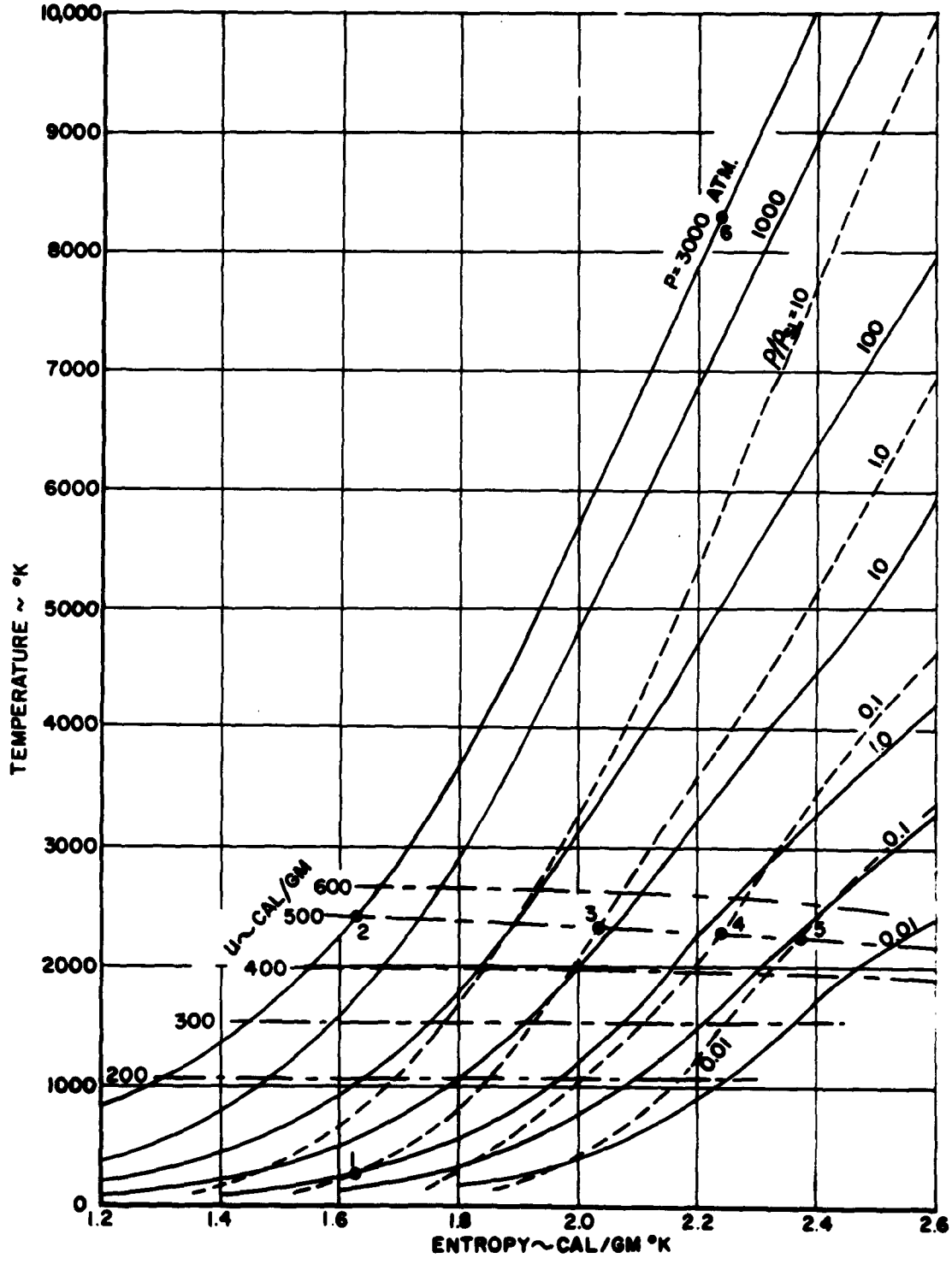

Figure 29 Thermodynamic Properties of High Temperature Air.

A. TAPERED TUBE INTERFACE STABILITY STUDY

The theoretical analysis, presented in Reference 1, of the interface velocity, of a liquid driver compressing a charge of gas in a closed end tapered tube, was based upon the equations of conservation of mass and momentum for one dimensional, incompressible, unsteady flow. If a tapered tube of fixed configuration is to stabilize a liquid-gas interface, the question arises at what point in the tube will this stability break down for a given driver pressure. If it is assumed that this point occurs when the interface acceleration is zero, i.e., $dq_i/di = 0$, the location can be determined from Eqs (86), (91) and (95) from Reference 1. In order these equations are:

$$\frac{dq_i}{di} + \left(\frac{1}{A(i) \int_0^i \frac{dx}{A(x)}} + \frac{2}{A(i)} \frac{dA(i)}{di} \right) qi = \frac{P_d - P_c}{A(i) \int_0^i \frac{dx}{A(x)}} , \tag{38}$$

$$P_c = P_o \left(1 - \frac{V_i}{V_o} \right)^{-n} , \tag{39}$$

and

$$\bar{q}_i = \frac{V_i}{\left[A(i) \right]^2 \int_0^i \frac{dx}{A(x)}} \left(\pi_d + \frac{1 + \pi_c^{\frac{n-1}{n}}}{(n-1)(1 - \pi_c^{-1/n})} \right) \tag{40}$$

where x is the variable length from the entrance of the tapered tube and i is the interface location from the same reference. Equating dq_i/di to zero and combining Eqs (38), (39) and (40) the position at which the interface becomes unstable, for a given drive r pressure, can be determined from the result, which is

$$\pi_d = \frac{\left[\frac{V_i}{\left[A(i) \right]^2 \int_0^i \frac{dx}{A(x)}} + \frac{2V_i}{\left[A(i) \right]^2} \frac{dA(i)}{di} \right] \left[\frac{(1 - V_i/V_o)^{1-n} - 1}{(n-1) V_i/V_o} \right] - (1 - V_i/V_o)^{-n}}{\left(\frac{V_i}{\left[A(i) \right]^2 \int_0^i \frac{dx}{A(x)}} + \frac{2V_i}{\left[A(i) \right]^2} \frac{dA(i)}{di} \right) - 1} . \tag{41}$$

If a shape for the tube is assumed, the location of the interface, at which it becomes unstable, can be determined as a function of the driver pressure ratio from Eq(41). Once this location is determined the value of the charge gas pressure ratio at break down π_{bd} can be calculated from Eq (39) and the value of the peak pressure π_m can be calculated from Eq (40) if $\bar{q}_i$ is set equal to zero. Finally, for a given configuration, a curve of the ratio π_{bd}/π_m versus

π_d can be obtained. This has been accomplished for the case of a linear area change tube and n = 1.31, and is plotted in Figure 30; the data for this plot is given in Table VI. The significant equations needed for this configuration are:

$$\frac{dA(i)}{di} = - S, \tag{42}$$

$$A(i) = A_e - Si, \tag{43}$$

$$V_i = \frac{A_e + A(i)}{2} i, \tag{44}$$

$$\int_0^i \frac{dx}{A(x)} = - \frac{1}{S} \ln(A(i)/A_e). \tag{45}$$

Using Eqs (42) through (45) with Eq (41) and letting $Y = A_e/A(i)$ yields,

$$\pi_d = \frac{(1 - \ln Y^2)\left(\frac{Y^{2(n-1)} - 1}{n - 1}\right) Y^2 + Y^{2n}}{1 + (1 - 1/\ln Y^2)(Y^2 - 1)} \tag{46}$$

TABLE VI

Data for Figure 30

1/Y	Y	i_{bd}/ℓ_t	π_{bd}	π_d	π_m	π_{bd}/π_m
.5	2.0	.5	6.15	4.39	37.9	16.2%
.4	2.5	.6	11.0	5.32	62.0	17.7
.3	3.33	.7	23.4	6.76	119	19.6
.2	5.0	.8	68.0	9.32	315	21.6
.1	10.0	.9	415	15.5	1700	24.4
.05	20.0	.95	2590	25.2	10,000	25.9

B. TAILORED TUBE PROBLEM

A solution to a problem of tailoring a liquid to gas compression tube to have a constant interface velocity was suggested by Dr. Hans J. P. von Ohain and was developed as follows utilizing the following assumptions:

(a) A "long" driver tube precedes the tailored compression chamber so that:

(1) The compression signals will not be reflected and return to the compression chamber before the process is completed and

(2) the kinetic energy is large compared to the work of compression of the gas.

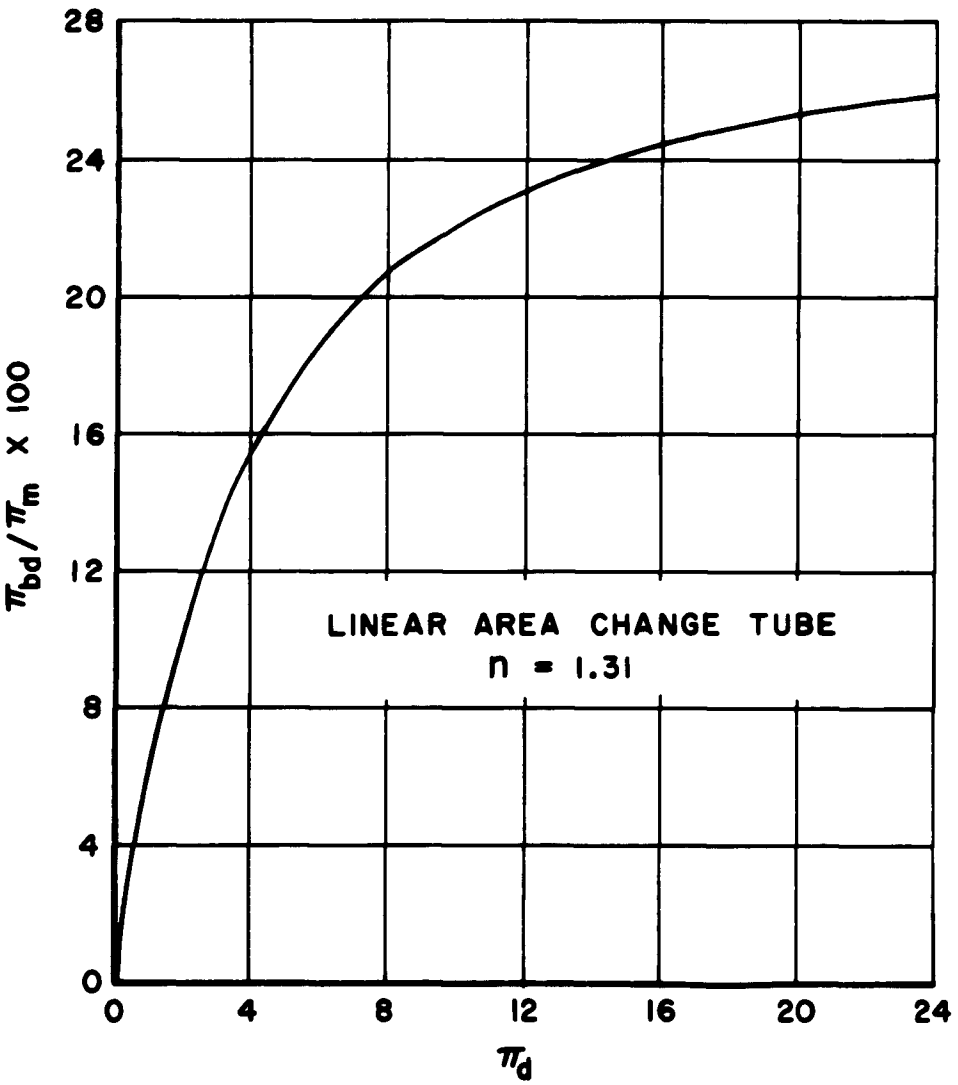

Figure 30 Charge Gas Pressure at Interface Break Down in Percent of Maximum Charge Gas Pressure Versus Driver Pressure Ratio for a Tube in which the Area Decreases Linearly with Length.

(b) The flow is one dimensional.

(c) The speed of sound, s, in the liquid is constant.

(d) Friction is neglected.

(e) All the kinetic energy of the liquid is converted to strain energy in the liquid,
i.e. $dP = -\rho\, s\, du$,
where the Δu is the change of velocity of the liquid in the long tube. (This assumption is essentially identical to (a2) above.)

(f) The pressure at the interface (hence in the gas) is a function of the instantaneous chamber volume,

i.e. $dP_c = dV \frac{dP_c}{dV}$

(g) The signaling speed is almost instantaneous so that the assumption of the incompressibility of the liquid can be utilized in the continuity equation,

i.e. $u_\ell\, \rho_\ell A_e = u_o \rho_\ell A(x)$.

Thus

$$A_e du_\ell = u_o dA(x)$$

or

$$du_\ell = \frac{u_o}{A_e}\, dA(x).$$

Combining the above with the condition that the pressure in the gas and the liquid are equal at the interface,

$$dP_c = dP_\ell = -\frac{u_o}{A_e}\, \rho_\ell\, s\, dA(x)$$

or

$$P_c - P_o = -\frac{u_o \rho_\ell s}{A_e}\, (A(x) - A_e). \tag{47}$$

Equation (47) is independent of the particular pressure function in the gas, however, the actual shape of the chamber cannot be determined until the gas pressure is known as a function of the variable length x.

Now if it is assumed that the gas is compressed polytropically we have

$$P_c = P_o \left(\frac{V_o}{V}\right)^n , \tag{48}$$

$$\left(\frac{V_o}{V}\right)^n - 1 = \frac{u_o \rho s}{P_o}\left(1 - \frac{A(x)}{A_e}\right),$$

now

$$dV = -A(x)dx, \text{ or}$$

$$-A(x) = \frac{dV}{dx},$$

$$\left(\frac{V_o}{V}\right)^n - 1 = \frac{P_{wh}}{P_o}\left(1 + \frac{V_o}{A_e}\frac{d\frac{V}{V_o}}{dx}\right), \text{ and}$$

$$V_i = \int_0^i A(x)dx.$$

Thus

$$\frac{V}{V_o} = 1 - \frac{V_i}{V_o}$$

$$\left(1 - \frac{V_i}{V_o}\right)^{-n} - 1 = \frac{P_{wh}}{P_o}\left(1 - \frac{d\left(\frac{V_i}{V_o}\right)}{d\left(\frac{A_e}{V_o}\right)x}\right)$$

Defining the dimensionless ratios

$$\nu = \frac{V_i}{V_o}$$

$$X = \frac{A_e}{V_o}x = \frac{x}{\ell_e},$$

$$\pi_{wh} = \frac{P_{wh}}{P_o},$$

we have

$$X = \int_o^\nu \frac{\pi_{wh} d\nu}{(\pi_{wh}+1)-(1-\nu)^{-n}}. \qquad (49)$$

Eqs (48) and (49) were programmed for a digital computer and solutions obtained for various values of π_{wh} and n.

In the construction of any real equipment utilizing Eqs (48) and (49) the design must insure that the assumptions used in obtaining them are valid.

For the length of the driver tube ℓ_t (not including the compression chamber) necessary to satisfy assumption (a1) (signaling time) we have the following:

compression time t_c is given by

$$t_c \doteq \frac{\ell_e}{u_o},$$

and signaling time t_s is

$$t_s = \frac{2\ell_t}{s}$$

To satisfy (a1), $t_s \geq t_c$. Using the equality we have

$$\left(\frac{\ell_t}{\ell_e}\right)_s \geq \frac{1}{2} \frac{s}{u_o} . \tag{50}$$

The energy assumptions (a2) and (e) require that the energy ratio $R = KE/WK_c$ be large. This can be formulated:

$$KE = \frac{1}{2} \rho_\ell u_o^2 A_t \ell_t,$$

$$WK_c = \frac{1}{n-1} P_o V_o (\pi_{wh}^{\frac{n-1}{n}} - 1),$$

$$R = \frac{(n-1)\rho_\ell u_o^2}{2P_o (\pi_{wh}^{\frac{n-1}{n}} - 1)} \left[\frac{A_t \ell_t}{A_e \ell_e},\right]$$

$$\left(\frac{A_t \ell_t}{A_e \ell_e}\right)_E = \frac{2(\pi_{wh}^{\frac{n-1}{n}} - 1)}{(n-1)\pi_{wh}} R. \frac{s}{u_o} \tag{51}$$

To satisfy assumption (b) (1 dim. flow) the angle from the horizontal should be equal to or less than 20^o (arbitrary choice). From the numerical data (and the mean value theorem from calculus) we have

$$\frac{1}{2}\,\frac{d_1 - d_2}{x_2 - x_1} \leq \tan 20^\circ \doteq .36$$

$$\frac{\dfrac{d_1}{d_e} - \dfrac{d_2}{d_e}}{\dfrac{x_2}{\ell_e} - \dfrac{x_1}{\ell_e}}\,\frac{d_e}{\ell_e} \doteq .72$$

$$\frac{\ell_e}{d_e} \doteq 1.4\,\frac{\dfrac{d_1}{d_e} - \dfrac{d_2}{d_e}}{\dfrac{x_2}{\ell_e} - \dfrac{x_1}{\ell_e}} \tag{52}$$

Therefore given π_{wh}, n and the value of the pressure one wishes to achieve before the one dimensional assumption breaks down and ratio ℓ_e/d_e can be determined.

Assumptions (c), (f) and (g) are considered to be justified in the range of values of pressure and temperature considered.

The friction may not be negligible, however, in early stages of compression the chamber can be tailored to nullify the frictional effects. Also, the actual conditions prevailing at the instant the liquid reaches the chamber entrance would determine u_o and hence the frictional effects of the tube are accounted for.

Eq (51) determines the volume ratio for a given R, but if the area of the tube is assumed to be constant and equal to the initial area of the chamber A_e then Eq (51) determines the length ratio for a given R. Tables VII and VIII give comparisons of Eqs (50) and (51).

In Table VII the length determined by Eq (51) is compared to the length determined from Eq (50), i.e. $(\ell_t/\ell_e)_E/(\ell_t/\ell_e)_s$.

TABLE VII

Values of $(\ell_t/\ell_e)_E/(\ell_t/\ell_e)_s$

π_{wh}	R = 100, n = 1.4 $(\ell_t/\ell_e)_E/(\ell_t/\ell_e)_s$	R = 100, n = 1.2 $(\ell_t/\ell_e)_E/(\ell_t/\ell_e)_s$
1000	6.2	4.20
1500	4.72	3.30
2000	3.9	2.54
2500	3.36	2.14
3000	2.96	1.87
4000	2.44	1.49
5000	2.08	1.26

In Table VIII the value of R is given for the case where ℓ_t/ℓ_e is determined by Eq (50).

TABLE VIII

Values of R if $\ell_t/\ell_e = (\ell_t/\ell_e)_s$

π_{wh}	n = 1.4 R	n = 1.2 R
1000	16.1	23.4
1500	21.2	30.3
2000	25.6	39.4
2500	29.8	46.6
3000	33.8	53.5
4000	41.0	67.0
5000	48.0	79.4

C. MEMBRANE SEPARATION STUDY

It was suggested in conjunction with tapered tubes and liquid driver fluids, by Dr. Hans J. P. von Ohain of the Aerospace Research Laboratory, that membrane pistons might be employed to serve as a means of maintaining a stable interface between the liquid driver and charge gas and at the same time negotiate tapered tubes. To determine the feasibility of this concept a simple experimental system was constructed. This system, shown schematically in Figure 31, was constructed from clear acrylic plastic to allow photographic observation of the membrane piston.

During the compression process the piston travels first 51-1/4 inches in a 1 inch internal diameter acrylic tube, then negotiates a transition section 17-1/2 inches long in which the internal diameter varies linearly from 1 inch to 1/2 inch. Upon emerging from the transition section the piston travels in a 1/2 inch internal diameter acrylic tube until the charge gas is compressed to peak pressure.

The pistons which have been tested thus far were constructed from aluminum foil. Shown on the left of Figure 32 is a piston before use and on the right side of the same photograph is shown a piston after the compression process.

High speed motion pictures have been obtained for a number of compressions with the membrane pistons. These pictures have demonstrated that the piston is able to smoothly negotiate the transition section and seal the liquid driver provided the diaphragm ruptures properly. These tests, however, were performed with low values of driver pressure because of the low structural strength of the plastic tubes.

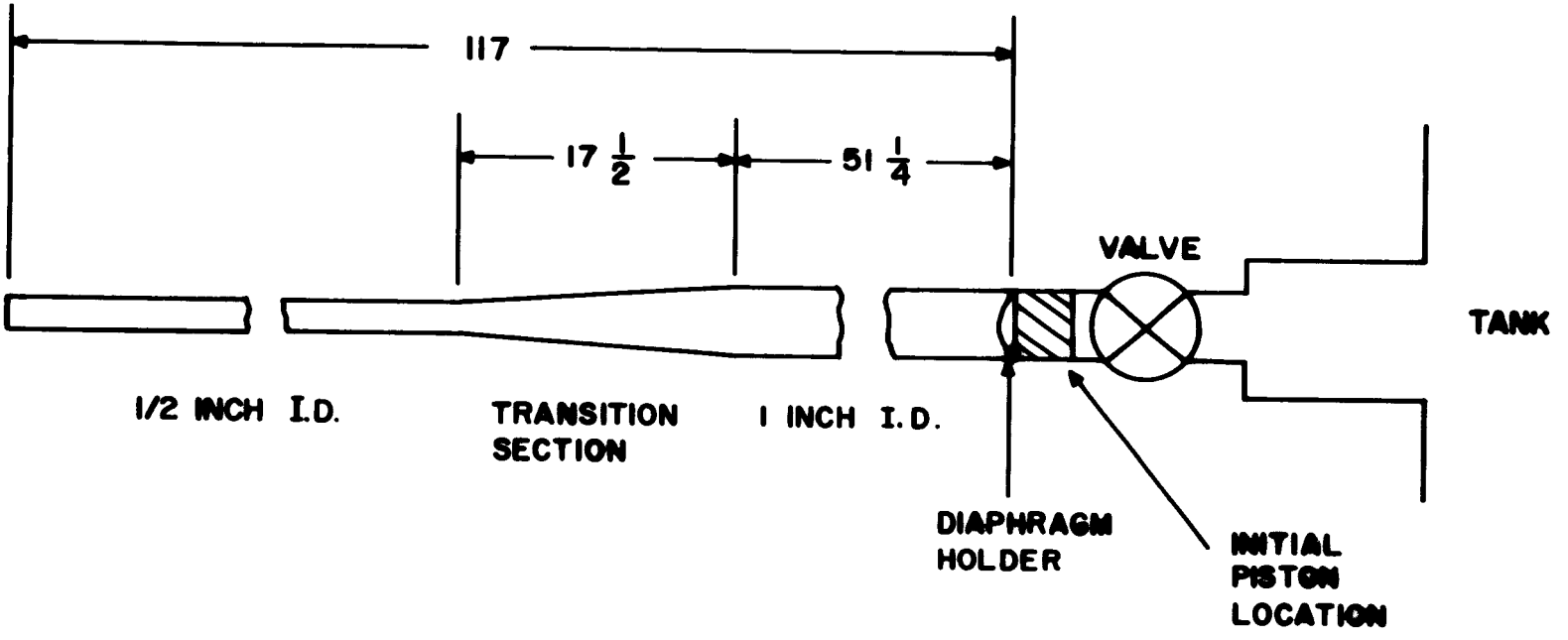

Figure 31 Schematic Diagram of Experimental System for Membrane Piston Study.

Figure 32 **Photograph of Aluminum Foil, Membrand Piston before and after a Test.**

REFERENCES

1. Minardi, J. E., and R. B. Schwartz. Research on Systems for Production of High Temperature and High Density Gases. ARL 62-398, July 1962.

2. Stalker, R. J. "Isentropic Compression of Shock Tube Driver Gas." ARS Journal, June 1960.

3. Bray, K. N. C. An Evaluation of the Hypersonic Gun Tunnel. International Hypersonics Conference, American Rocket Society Paper 1971-61, August 1961.

4. East, R. A., and L. Pennelegion. The Equilibrium Piston Technique for Gun Tunnel Operation. Aeronautical Research Council Report No. A. R. C. 22,852 Hyp. 186, April 1961.

5. Evans, C., and F. Evans. "Shock Compression of a Perfect Gas." Journal of Fluid Mechanics, October 1956, p. 399.

6. Roshko, A., and M. Rubinstein. Tables of Flow Functions for a Simple Non-Steady Expansion Wave. Douglas Aircraft Company Report No. ES 40031, September 1960, ASTIA Document No. 246728.

7. Lemcke, B. An Investigation of the Stagnation Conditions in the Shock-Compression Heater of a Gun Tunnel. The Aeronautical Research Institute of Sweden Report 90, February 1960.

8. Glass, I. I., and J. G. Hall. Handbook of Supersonic Aerodynamics, "Section 18, Shock Tubes." NAVORD Report 1488 (Vol. 6).

9. Ryabinin, Y. N. Gases at High Densities and Temperatures. London, Pergamon Press, 1961. A translation of "Gazy pri bol'shikh plotnostyakh i vysokikh temperaturakh," Moscow, Fizmatgiz, 1959.

Aerospace Research Laboratories, Wright-Patterson Air Force Base, Ohio. INVESTIGATIONS OF BALLISTIC-PISTON AND LIQUID DRIVEN PISTON COMPRESSORS FOR THE PRODUCTION OF HIGH TEMPERATURE AND HIGH DENSITY GASES by J. E. Minardi, R. B. Schwartz. August 1963. 75 p. incl illus and tables. (Project 7116; Task 7116-01) Contract AF 33(657)-8975 (ARL 63-167).

Unclassified Report

Research on systems for the production of high temperature and high density gases is being conducted by the University of Dayton Research Institute to determine the feasibility of various pressure energy exchange apparatus to produce isolated high

(over)

temperature and high pressure gas. The subject of this technical note is the theoretical analysis and experimental test program conducted to gain insight into the operation of ballistic-piston compressors, and the continuation of effort toward the development of liquid driven gas compression systems.

Aerospace Research Laboratories, Wright-Patterson Air Force Base, Ohio. INVESTIGATIONS OF BALLISTIC-PISTON AND LIQUID DRIVEN PISTON COMPRESSORS FOR THE PRODUCTION OF HIGH TEMPERATURE AND HIGH DENSITY GASES by J. E. Minardi, R. B. Schwartz. August 1963. 75 p. incl illus and tables. (Project 7116; Task 7116-01) Contract AF 33(657)-8975 (ARL 63-167).

Unclassified Report

Research on systems for the production of high temperature and high density gases is being conducted by the University of Dayton Research Institute to determine the feasibility of various pressure energy exchange apparatus to produce isolated high

(over)

temperature and high pressure gas. The subject of this technical note is the theoretical analysis and experimental test program conducted to gain insight into the operation of ballistic-piston compressors, and the continuation of effort toward the development of liquid driven gas compression systems.